Neurobehavioral dynamics of drowsiness

Valdas Noreika[1,2,3], Marc R. Kamke[1], Andres Canales-Johnson[2,3], Srivas Chennu[4,5], Jason B. Mattingley[1,6], and Tristan A. Bekinschtein[2,3]

[1] Queensland Brain Institute, University of Queensland, St Lucia, QLD 4072, Australia
[2] Department of Psychology, University of Cambridge, Cambridge, CB2 3EB, United Kingdom
[3] Medical Research Council Cognition and Brain Sciences Unit, Cambridge, CB2 7EF, United Kingdom
[4] School of Computing, University of Kent, Medway, United Kingdom
[5] Department of Clinical Neurosciences, University of Cambridge, Cambridge, United Kingdom
[6] School of Psychology, University of Queensland, St Lucia, QLD 4072, Australia

Correspondence: Valdas Noreika, Department of Psychology, University of Cambridge, Downing Street, Cambridge CB2 3EB, UK. Phone: +44 7733 630122. E-mail: valnoreika@gmail.com (vn261@cam.ac.uk)

Acknowledgements: The study was supported by the Wellcome Trust (TAB), the EU International Research Staff Exchange Scheme -IRSES (TAB/JBM), the Australian Research Council (JBM) and the National Health and Medical Research Council (JBM).

Abstract

Drowsiness varies continuously during daily activities, influencing both efficiency of daily behavior and sleep initiation. Yet, brain and behavioral dynamics underlying wake-sleep transitions, leading to the loss of perceptual awareness, are largely unknown in humans. Across levels of drowsiness we measured muscle and brain responses as participants attempted to detect their own hand movements elicited by transcranial magnetic stimulation to the motor cortex. Sleep and loss of consciousness processes –motor reorganization and decreased information shared by the brain– emerged through early drowsy states while participants were still conscious and able to take decisions. These findings demonstrate flexible adaption of perceptual processes to the changing neural dynamics of sleep onset long before the loss of responsiveness, and provide a mechanistic explanation for sleepiness affecting daily performance.

Drowsiness frames our conscious life – from a desperate snoozing of the alarm clock early in the morning to an unintentional head nodding while reading a book in the late evening. Importantly, drowsiness also interferes with our daytime activities, such as when driving a car for a prolonged period of time, or pervasively in continuous tasks while at work, yielding huge economic and social burden(*1*–*3*). Such intrusions of sleepiness become increasingly common as individuals develop more hectic lifestyles with chronic sleep restriction(*4*–*6*). Furthermore, abnormalities in the control of drowsiness contribute to sleep onset disorders such as insomnia(*7*) and narcolepsy(*8*). Aforementioned examples of appropriate as well as adverse natural occurrences and clinical conditions reveal drowsiness as a transitional global state of decreased arousal. As such, drowsiness is likely to share neural processes specific to both wakefulness and light sleep; these are marked by rather dissimilar neurophysiological and behavioral processes that are poorly characterized during the transition(*9*) and definitely not studied under a mechanistic framework.

It is known that tight control of the motor system and its continuous interaction with sensory networks in the awake state contrasts sharply with inhibition of motor processing during non-rapid eye movement (NREM) sleep, as evidenced by reduced motor cortex excitability(*10*) and the lack of voluntary movement during late sleep stage 1 (N1) and stage 2 (N2)(*11*). Furthermore, neural information complexity and effective connectivity diminish substantially during NREM sleep, while cortical reactivity and stereotypical processing of neuronal information are facilitated(*12*–*14*). Increased stereotypical local reactivity alongside with decreased global connectivity has been suggested to have a role in the suppression of conscious awareness during sleep(*13*, *15*, *16*). However, it remains elusive whether reorganization of these neural processes begins during early drowsiness when participants are still conscious and responsive, or if these changes only occur once they reach a certain 'tipping point' characterized by unresponsiveness(*9*). We also know little about the effect of such reorganization for sensory awareness. We aimed to shed light on these questions by unraveling the neural mechanisms and behavioral dynamics of drowsiness in human participants while consciously making perceptual decisions but slowly drifting into sleep.

In this study, we developed a novel experiment to assess participants' capacity to detect their hand muscles moving (kinesthetic awareness) and the associated neural mechanisms in the transition from wakefulness to sleep. Unlike most sensory detection/discrimination tasks in cognitive neuroscience where the stimuli are directly applied to the sensory organs, in this case we applied an electromagnetic pulse to the motor cortex of the participants for them to detect if their hand had moved. Specifically, we studied physiological and behavioral responses to TMS applied to the motor cortex at different levels of spontaneously fluctuating daytime arousal. Participants (N=20, mean age 23.7) were allowed to fall asleep while their hand representation area in the right motor cortex received single pulse TMS at 9 different intensities centered on their individual motor thresholds. Following each TMS pulse, participants responded with the non-stimulated right hand to indicate whether they felt

something in the stimulated hand or not (Fig. 1A-B) (see also Table S1).

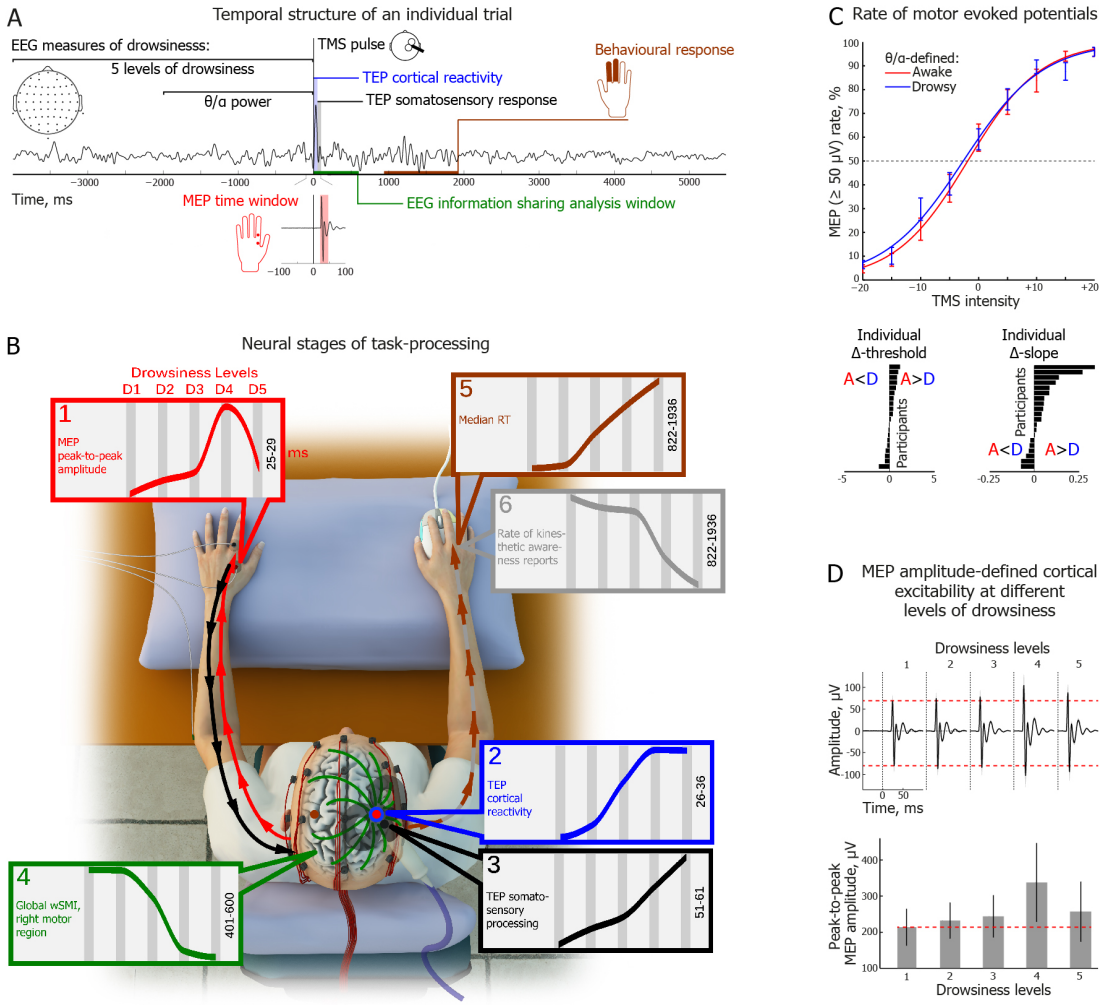

Fig. 1. Experimental design and key stages of task-related neural processing in different levels of drowsiness. (A) Temporal structure of an individual trial. Two EEG windows preceding single pulse TMS were used to assess drowsiness. Following TMS over the right motor cortex, motor evoked potentials (MEPs) were recorded from the first dorsal interosseous (FDI) muscle of the left hand (red). The participant reported if they felt something in their left hand by pressing one of the two mouse buttons with their right hand. Individual medians of reaction times ranged from 822ms in Drowsiness Level 1 to 1936ms in Level 5 (brown). TMS-evoked potentials (TEP) were analyzed in the 0-100ms post-TMS time window (blue and black), whilst EEG information-sharing in 0-600ms (green). **(B)** Key stages of TMS-triggered neurobehavioral processing across 5 levels of drowsiness (grey bars in the color insets). Interpolant function is fitted to the raw measurements at each Drowsiness Level. Time window of each stage of processing is indicated on the right side of each inset. Single pulse TMS over the right motor cortex evoked motor efferent signal (red arrow along the left arm), measured as a nonlinear MEP response from the FDI muscle (red inset). Concurrently, TEP was recorded at the site of stimulation (blue inset). An FDI muscle twitch in the left hand would send afferent kinesthetic signals (black arrow along the left arm), peaking in TEP brain activity posterior to the site of stimulation (black inset). EEG channel connectivity (green lines across the scalp, 0-600ms time window) calculated as global weighted symbolic mutual information (wSMI) index post-TMS (green inset) showed a sigmoidal

decrease with drowsiness. Following kinesthetic awareness decision, the response delivered by the contralateral motor efferent signal (brown-grey arrow along the right arm) showed different dynamics between median RT (brown inset) and the rate of kinesthetic awareness reports (grey inset). **(C)** Group-averaged rate of trials with MEPs above threshold value of 50μV across 9 TMS intensities, centered on individual motor threshold (0%). Sigmoidal functions are fitted separately to the θ/α-defined awake (red) and drowsy (blue) conditions (I-bars represent standard error of mean, SEM). Insets at the bottom depict each participant's sigmoid threshold and slope difference (Awake-Drowsy) (horizontal bars sorted in ascending order). Only responsive trials are included in the analysis shown in this and other subplots. Arousal states are distinguished here using EEG θ/α measure of 2000-0ms pre-TMS pulse. **(D, top)** Group-level dynamics of MEP across Drowsiness Levels 1-5. Horizontal red dashed lines delineate peaks at 25 and 29ms post TMS (0ms) in Drowsiness Level 1. **(D, bottom)** Change of the MEP peak-to-peak amplitude across Drowsiness Levels 1-5; I-bars represent SEM.

Table S1. Subjective reports of TMS-induced sensations.

Participant	Please describe any sensations that you felt in your left hand from the TMS
1	Tightness of muscle when my thumb twitched.
2	Short 'pins and needles' feeling. When thumb moved – sharper sensation.
3	Twitching and movement of individual fingers (including thumb), movement of the whole hand. Tension of the muscles.
4	Normal reflex.
7	Twitching.
8	Twitching of my left hand and small muscle movements around my fingers.
9	Slight twitch.
10	Twisting and tingling.
11	Moving by itself, like touching an electric fence.
12	Twitch on the fingers and forearm.
14	Itches, muscle movements.
15	Mostly light muscle movements.
16*	Just touching sensations, very soft most times.
17	Twitching.
18	Felt like my left hand was sometimes moving not voluntarily.
19	Fingers moving / contraction.
20	Sometimes something like tension, movement.

Note. * Participant 16 was the only one who conceptualized their experiences as primarily tactile. Notably, this participant had the lowest resting motor threshold (34%) of the whole sample.

By assessing the level of arousal on a trial-by-trial basis before each TMS pulse, we were able to track how instantaneous drowsiness modulates the chain of

neural and behavioral processes elicited by the TMS perturbation (Fig. 1A-B). This experimental paradigm allowed us to follow, with mechanistic detail, the path of the neural information signal travelling from the cortex to the hand and back to the cortical sensory processing, followed by perceptual decision and accuracy of kinesthetic awareness response. We specifically assessed: (1) motor excitability as measured by peripheral motor evoked potentials (MEPs) from the stimulated hand (25-29ms); (2) concurrent local cortical reactivity as measured by TMS-evoked potentials (TEPs) (26-36ms); (3) somatosensory processing of TMS-triggered sensations as measured by somatosensory evoked potentials (SEPs) (51-61ms); (4) long range cortical information sharing (0-600ms); (5) the speed of neurobehavioral processing as measured by the reaction times (RT; >800ms); and (6) kinesthetic awareness as measured by the rate of perceived movement reports (>800ms).

We first assessed motor excitability as a function of drowsiness. Motor excitability, as measured by the peripheral MEP in response to cortical TMS, tends to decrease with increasing sleepiness due to homeostatic and circadian effects(*17*, *18*), although the findings are often inconsistent(*19*, *20*). Arguably, different levels of arousal (the complexity of the transition to sleep), averaged into a single sleep state could explain the lack of consistency. Leaving behind the assumption of a steady state of arousal, we measured the continuous changes during the transition to sleep at a single trial level, allowing a more fine-grained measurement of drowsiness. A two-fold representation of the EEG level of arousal was applied over the time window preceding TMS: (1) categorical definition of awake and drowsy states following EEG spectral power signatures (θ/α) averaged across all EEG electrodes(*21*), and (2) dynamical definition of 5 levels of drowsiness following the Hori system for scoring of sleep onset(*22*) (Fig. S1).

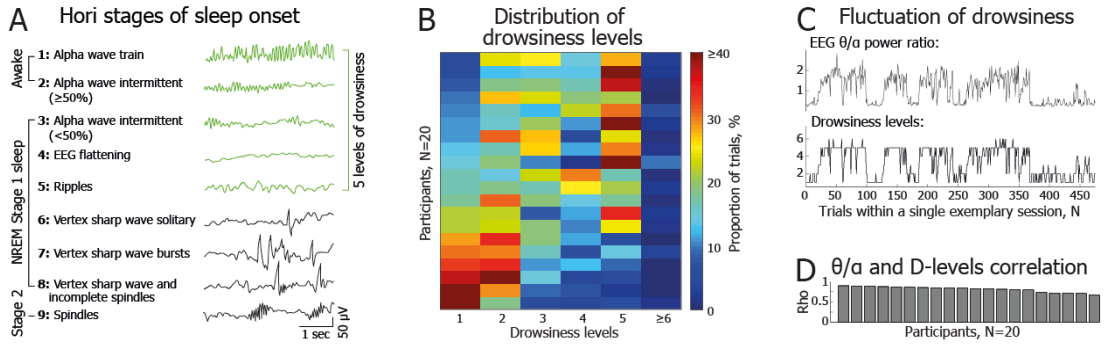

Fig. S1. Electroencephalography (EEG) measures of drowsiness. (A) Brief definitions and EEG examples of 9 Hori stages of sleep onset, progressing from relaxed wakefulness(Hori Stage 1) to NREM Stage 2 sleep (Hori Stage 9) (modified with permission from(*23*)). In the current study, Drowsiness Levels 1-5 (marked in green) correspond to Hori Stages 1-5. These were manually scored using 4-second EEG segments preceding TMS. **(B)** Percentage of trials scored as different Drowsiness levels within each participant (N=20). Datasets are sorted here from the most alert participants 1-2 with the dominance of Drowsiness Level 1 (bottom lines) to the drowsiest participants 18-20 with the dominance of Drowsiness Level 5 (top lines). There were very few epochs of Drowsiness Level 6 and above. **(C)** A representative

dataset of one participant with good agreement between the two EEG measures of drowsiness across the whole testing session. The top subplot indicates θ/α ratio, whereas the bottom subplot shows fluctuation of Drowsiness Levels. **(D)** Intra-individual correlations between θ/α power and Hori measures of drowsiness. Cross-validation of drowsiness: bars represent intra-individual Spearman's rank order correlation coefficients for 20 participants, sorted from the most to the least positive coefficients. A strong convergence between θ/α and Hori measures were observed for each participant.

To examine the association between muscle responsiveness (MEP) and arousal as a function of TMS intensity, we calculated the proportion of trials with MEP peak-to-peak amplitude above 50μV threshold in each of the 9 TMS intensities, separately for the θ/α-defined awake and drowsy trials. A sigmoid function was then fitted across arousal conditions to each participant. The slope of MEP sigmoid showed a small but reliable decrease in drowsiness compared to awake state (Wilcoxon signed-rank test: z-score=2.02, p=0.044, r=0.32), suggesting increased noise and instability in neural processing (see Fig. 1C and Fig. S2). Contrary to this, the MEP sigmoid threshold did not differ between awake and drowsy trials ($t_{(19)}$=1.31, p=0.21, d=0.13, Bf in favor of the null=2.04). We considered whether the observed difference in slope was specifically related to arousal, as the amplitude of pre-stimulus alpha oscillations has also been implicated in the fluctuation of attention and sensory gating. However, given that the observed difference of slope as a function of EEG θ/α power was temporally and spatially widespread (Fig. S3), contrary to more restricted effects of attention and sensory gating previously reported(*24–26*), we concluded that our results were mostly likely due to the shift from awake to drowsy states of arousal.

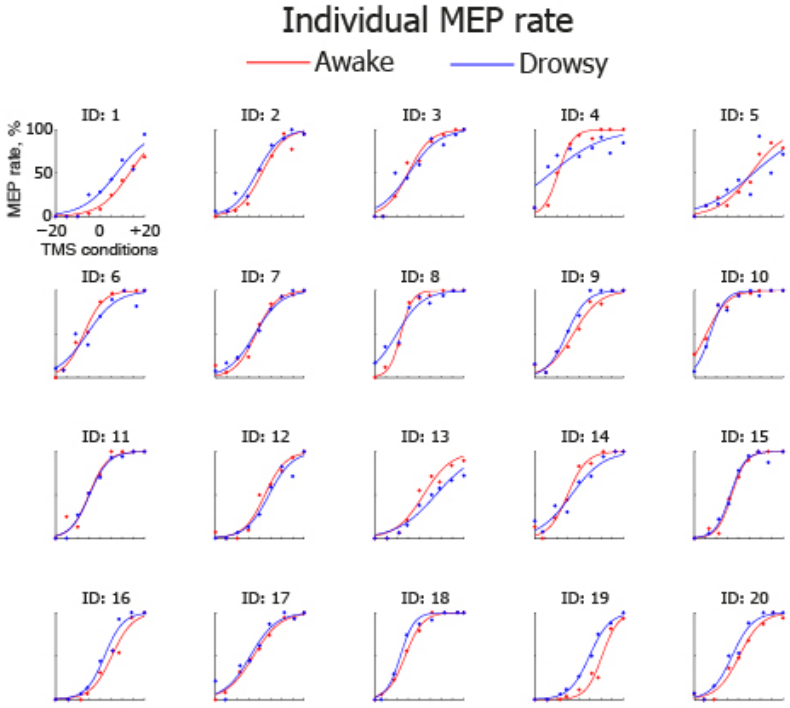

Fig. S2. Individual rate of motor evoked potentials (MEPs) as a function of transcranial magnetic stimulation (TMS) intensity in θ/α-defined awake and drowsy states. Percentage of trials with MEP potentials above threshold value of 50μV was calculated separately for the awake and drowsy trials across 9 TMS conditions centered on individual motor threshold (0%). Sigmoidal functions were then fitted to the awake (red) and drowsy (blue) conditions separately for each individual (N=20).

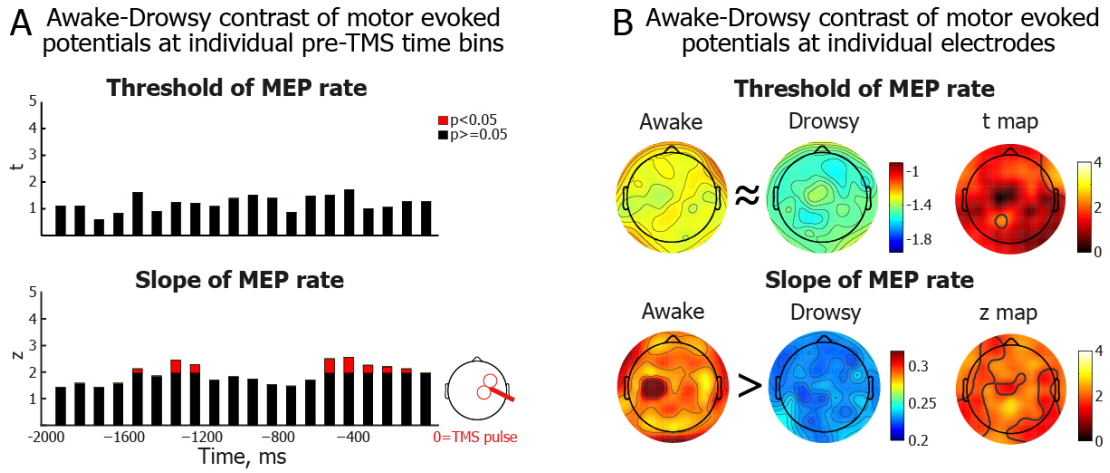

Fig. S3. Temporal and spatial spread of the arousal-dependent modulation of motor evoked potentials. (A) Difference of the motor evoked potential (MEP) sigmoid thresholds (top) and slopes (bottom) between θ/α-defined awake and drowsy conditions. Arousal states are measured and contrasted separately for each of the 20 time bins in steps of 100ms across the -2000-0ms pre-stimulation time window. Electroencephalography (EEG) spectral power is averaged over all electrodes. **(B)** Difference of the MEP sigmoid thresholds (top) and slopes (bottom) between θ/α-defined awake and drowsy conditions. Arousal states are measured and contrasted separately for each of the 63 EEG electrodes. EEG spectral power is averaged over -2000-0ms pre-stimulation time window.

We next compared MEP peak-to-peak amplitudes between Drowsiness Level 1, depicting relaxed wakefulness, and subsequent Levels 2-5, reflecting increasing levels of drowsiness. A reliable increase in MEP amplitude was observed between Levels 1 and 4 ($t_{(19)}$=3.5, p=0.0096, d=0.64), with an intermediate stepped increase in Levels 2 (d=0.15) and 3 (d=0.23) and a subsequent decrease in Level 5 (d=0.27) (see Fig 1D). A linear trend of increasing MEP amplitude was observed across Drowsiness Levels 1-4 ($F_{(1,19)}$=11.55, p=0.003, partial η^2=0.38), but not when all Levels 1-5 were considered ($F_{(1,19)}$=2.11, p=0.165, partial η^2=0.1). These findings indicate a non-linear reorganization of motor cortex excitability taking place at a time when drowsy participants are still conscious and responsive. The most noticeable change in dynamics occurs with the disappearance of alpha waves from the EEG (with EEG flattening and the first occurrence of EEG theta-range ripples - Levels 4 and 5), while participants are still responding. This suggests a much earlier modulation of excitability than previous reports of increased MEP with sleep deprivation or during NREM sleep(*10*, *17*, *18*), and highlights a much faster rate of cortical excitability

fluctuations.

We next assessed post-TMS cortical reactivity measured as TEP within the first 40ms. The early TEP amplitude is known to increase in response to homeostatic sleep pressure(*27*) and during NREM sleep(*14*), likely reflecting a combination of synaptic strengthening, changes in neuromodulation, and impaired inhibition(*27*). We hypothesized that, similarly to MEP amplitude, cortical reactivity would also depend on the trial-per-trial level of arousal in drowsy yet responsive participants.

First, TEP amplitude contrast between θ/α-defined awake and drowsy trials showed a reliable increase of cortical reactivity (larger TEP amplitude in drowsy) in the early 26-36ms peak ($t_{(19)}$=4.02, p=0.00074, d=0.49) (see Fig 2A) (consistent in 18/20 participants, see Fig. S4). While displaying a wide fronto-central spread, the peak differences between awake and drowsy states was in the right motor region right below the TMS coil (see Fig 2B-C). Additional control analyses confirmed that the observed TEP increase in drowsiness is not due to TMS-evoked scalp muscle artifacts (see Fig S5). We further compared TEP amplitude at the site of stimulation between Drowsiness Levels 1-5. As hypothesized, TEP amplitude increased nonlinearly across Drowsiness Levels following TMS (Mann-Kendall trend test: z=4.7, p=0.0000025, tau=0.77) (Fig 2D-E). Planned comparisons revealed a significant increase of TEP amplitude between Drowsiness Level 1 and Level 3 ($t_{(19)}$=4.54, p=0.00088, d=0.5), 1 vs. 4 ($t_{(19)}$=4.38, p=0.00099, d=0.68), and 1 vs. 5 ($t_{(19)}$=3.43, p=0.0056, d=0.6). These findings provide the first direct evidence of an inverse association between cortical reactivity and arousal, suggesting again that sleep mechanisms intrude upon local cortical processing while participants are still able to make perceptual decisions. Furthermore, the effects are early in the sleep onset (Level 3), before the appearance of ripples or slow waves(*22*).

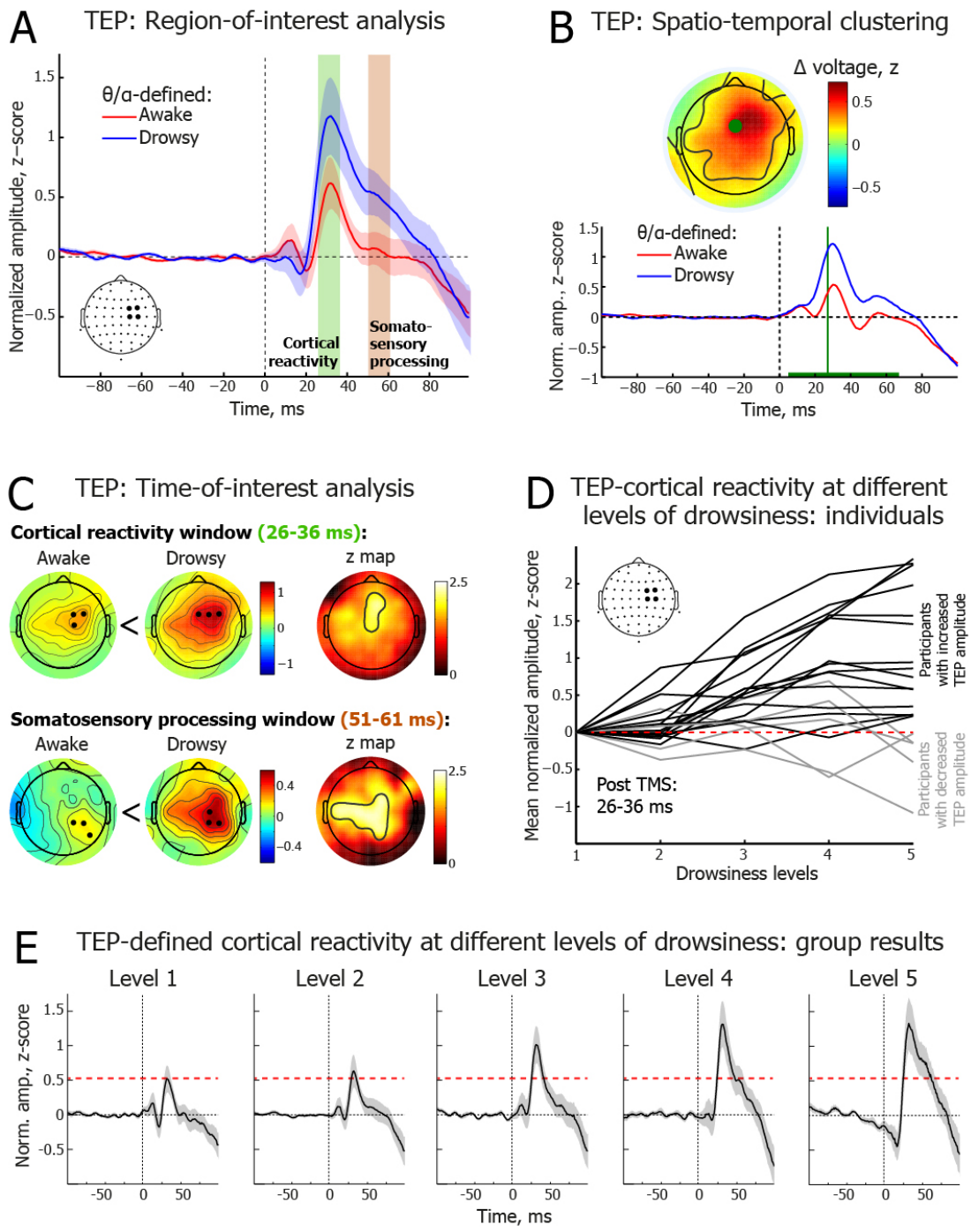

Fig. 2. Transcranial magnetic stimulation (TMS)-evoked cortical reactivity and somatosensory processing potentials in different states of arousal. (A) Time course of electroencephalography (EEG) potentials averaged over 4 EEG electrodes beneath TMS coil in the θ/α-defined awake (red) and drowsy (blue) states. Vertical bars highlight cortical reactivity (green, 26-36ms) and somatosensory processing (brown, 51-61ms) time windows. Only responsive trials are included in the analysis shown in this and other subplots. 0ms is TMS pulse time, error shades depict standard error of mean (SEM). **(B)** 0-100ms data-driven spatiotemporal clustering of EEG potentials post TMS between θ/α-defined awake (red) and drowsy (blue) states. Reliable differences where drowsy trials show higher positive TMS-evoked potentials (TEP) amplitude in the 5-67ms time window (cluster peak: 27ms, t = −4884.47, p = 0.004). The green horizontal line depicts the significant differences' time window. The largest difference

electrode waveform between arousal states electrode is marked as a green dot in the topographical voltage map. The black contours within the map reveal the electrodes with reliable differences (cluster). The topographical voltage map is at the peak difference between states. **(C)** Topographical distribution of the early TEP reflecting cortical reactivity (top, 26-36ms) and later somatosensory evoked potentials (SEPs; bottom, 51-61ms) peak latencies in the θ/α-defined awake (left) and drowsy (middle) states. Black dots indicate location of three EEG electrodes with the maximal amplitude in a given map, with a more posterior peak location in the somatosensory processing window. Non-parametric z maps (right) reveal regions reliably different between awake and drowsy states. **(D)** Individual-level dynamics of TEP cortical reactivity peak amplitude across Drowsiness Levels 1-5 (TEP amplitude averaged over 26-36ms across 4 electrodes beneath the TMS coil). Normalized amplitude is shown relative to Drowsiness Level 1 (red dashed line). Black lines represent participants with higher TEP amplitude in Drowsiness Level 5 compared to Level 1 (N=15); grey lines for participants with lower TEP amplitude in Drowsiness Level 5 compared to Level 1 (N=5). **(E)** Group-level dynamics of TEP waveforms across Drowsiness Levels 1-5 (TEP averaged over 4 electrodes beneath the TMS coil). Horizontal red dashed line delineates TEP cortical reactivity peak at 31ms post TMS in Drowsiness Level 1.

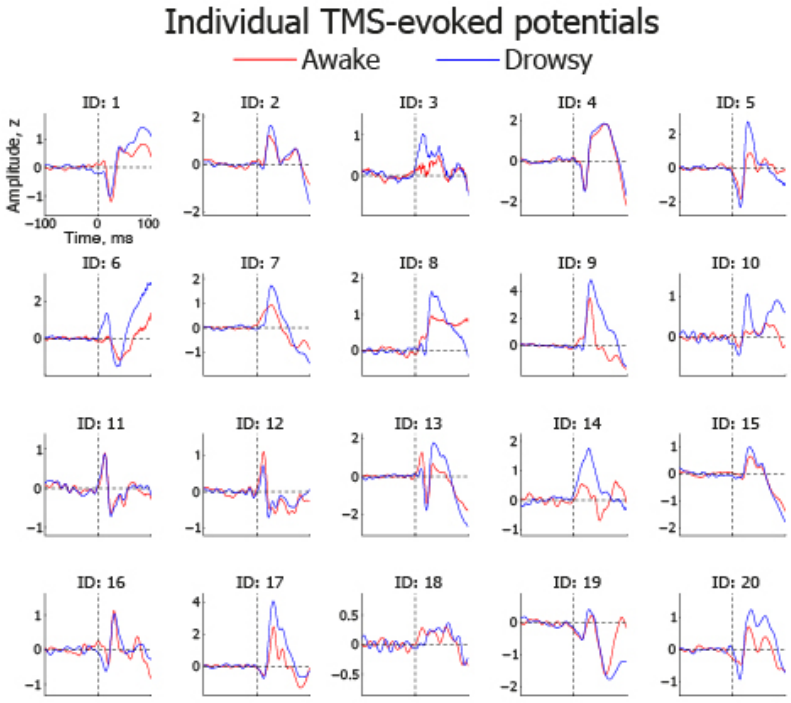

Fig. S4. Individual transcranial magnetic stimulation (TMS) evoked potentials (TEPs) in θ/α-defined awake and drowsy states. TEPs averaged across 4 EEG electrodes within a region-of-interest (ROI) beneath the TMS coil. Awake (red) and drowsy (blue) TEP waveforms are depicted separately for each individual (N=20).

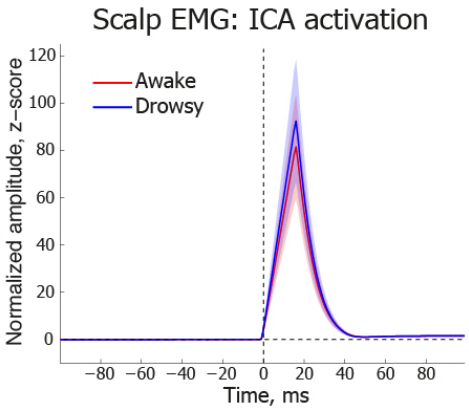

Fig. S5. TMS-evoked scalp muscle activity in θ/α-defined awake and drowsy states. Electromyography (EMG) waveforms depicting TMS-evoked scalp muscular contraction artifact identified during independent component analysis (ICA). After the identification of this component, trials were split between awake (red) and drowsy (blue) conditions. Data shown here are averaged across 16 participants who had this artifact. Error shades depict standard error of mean (SEM).

In addition to the early TEP centered under the TMS coil we hypothesized a somatosensory evoked potential (SEP) peak at a later time point, indicative of the return of the neural signal to the cortex from the hand (somatosensory stimulation due to TMS-induced muscle movement). Considering the ~27ms that the efferent signal takes to arrive at the hand muscles and ~20ms from the hand to the somatosensory cortex(*28*), the peak we observed at 51-61ms agrees with the arrival of an afferent somatosensory input to the cortex due to the experimental stimulation. Furthermore, the signal was posterior to the motor cortex stimulation site and following temporally the peak of the MEP (Fig. 2C). Moreover, and contrary to the early TEP, this SEP peak emerged only in the supra-threshold TMS conditions (+5% to +20%), when participants report awareness in most of the trials, corroborating the somatosensory origin of this SEP component (see Fig. S6). Similar to the early TEP, amplitude of SEP increased in the region-of-interest of the right hemisphere when participants became drowsy (Wilcoxon signed-rank test: z=2.98, p=0.003, r=0.47) (Fig. 2C).

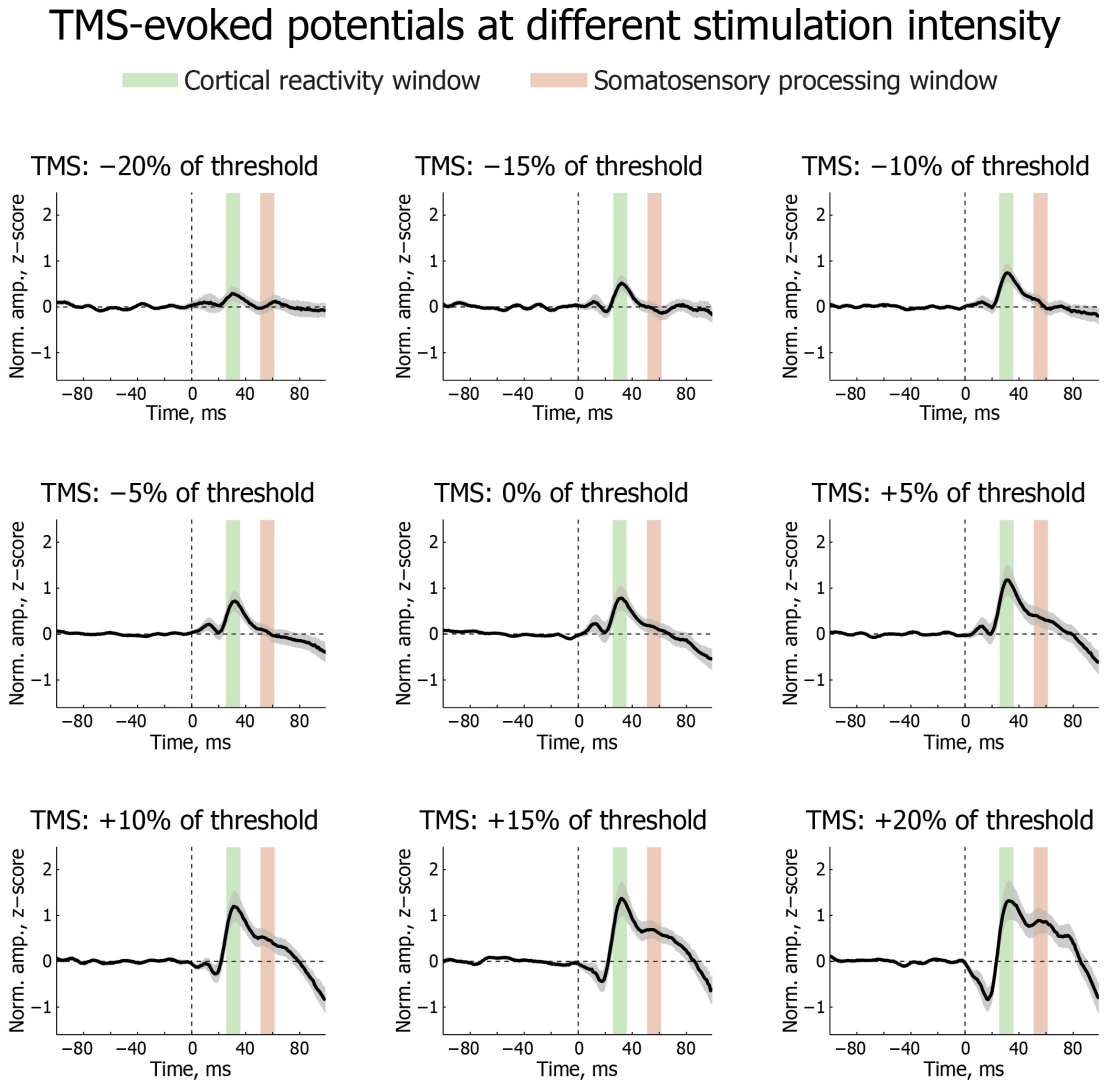

Fig. S6. Individual transcranial magnetic stimulation (TMS)-evoked potentials (TEPs) and somatosensory evoked potentials (SEP) as a function of TMS output intensity. TEPs and SEPs averaged across 4 EEG electrodes within a region-of-interest (ROI) beneath the TMS coil. Waveforms are shown separately for each of the 9 TMS output intensities centered on the individual motor threshold (0% condition). Green and brown vertical bars depict respectively cortical reactivity and somatosensory processing windows. Error shades represent standard error of mean (SEM).

After establishing effects of drowsiness on relatively early motor excitability, cortical reactivity and somatosensory processing, we investigated a broader time window that would encapsulate later stages of task-related processing. To address this, we first tested post TMS event-related potentials (ERP) and EEG connectivity patterns in the time window up to 600ms post-TMS. While a trend towards an increase of ERP amplitude was noticed in the left frontal region (around 200ms) and in the parietal region (around 300ms) during θ/α-defined drowsy compared to wake (Fig. S7), data-driven spatio-temporal ERP clustering in the 100-600ms time window revealed no reliable differences between awake and drowsy states.

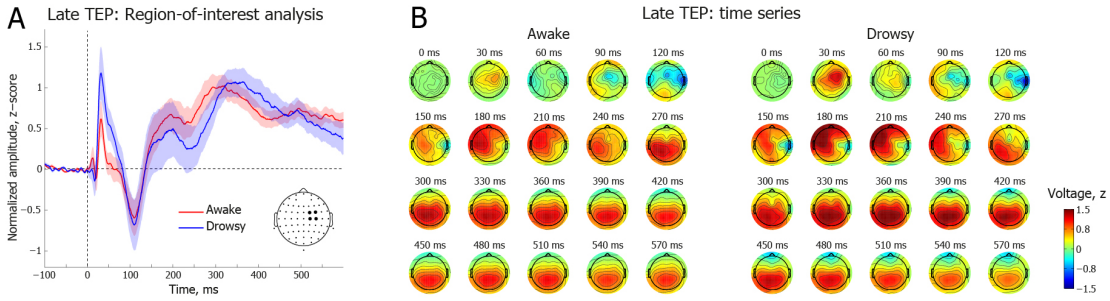

Fig. S7. Late TMS-locked event-related potentials (ERP) in θ/α-defined awake and drowsy states. (A) Time course of ERP waveforms averaged over 4 EEG electrodes beneath the TMS coil in the θ/α-defined awake (red) and drowsy (blue) states. TMS pulses were delivered at 0 ms. Error shades depict standard error of mean (SEM). **(B)** Topographic distribution of TMS-locked ERP in the θ/α-defined awake (left) and drowsy (right) states.

To assess how arousal modulates neural information processing we computed weighted symbolic mutual information index (wSMI), a measure of nonlinear information exchange between cortical sites, originally developed to discriminate between global states of consciousness(*29*, *30*) and recently adapted to study perceptual and cognitive processing(*31*, *32*). Given that EEG effective connectivity and coherence decrease during NREM sleep(*9*, *12–14*, *16*), we hypothesized that a similar decrease will occur in drowsiness, implying that wake-related long-range neural information sharing would start to disintegrate while drowsy participants are still conscious and responsive.

Clear global neural information exchange differences were observed between awake and drowsy trials in the post-TMS time window (Fig 3A and Fig S8). In particular, TMS perturbations triggered a sharp decrease in global wSMI on the ipsilateral motor region, which seemed sharper in drowsy compared to awake trials (0-200ms: $t_{(19)}$=2.02, p=0.057, d=0.4). Following the initial dip, the recovery from the informational disconnection was more efficient in awake than drowsy trials (200-400ms: $t_{(19)}$=2.73, p=0.026, d=0.63). Furthermore, global wSMI exceeded baseline levels in awake but not drowsy state in the late period (400-600ms: $t_{(19)}$=3.21, p=0.0138, d=0.94), indicating the facilitation of information sharing. Importantly, global wSMI was not different between states of arousal in the pre-TMS baseline period (-200-0ms) ($t_{(19)}$=1.48, p=0.16, d=0.11), confirming that arousal-specific information sharing differences emerged in response to TMS perturbation (Fig 3A).

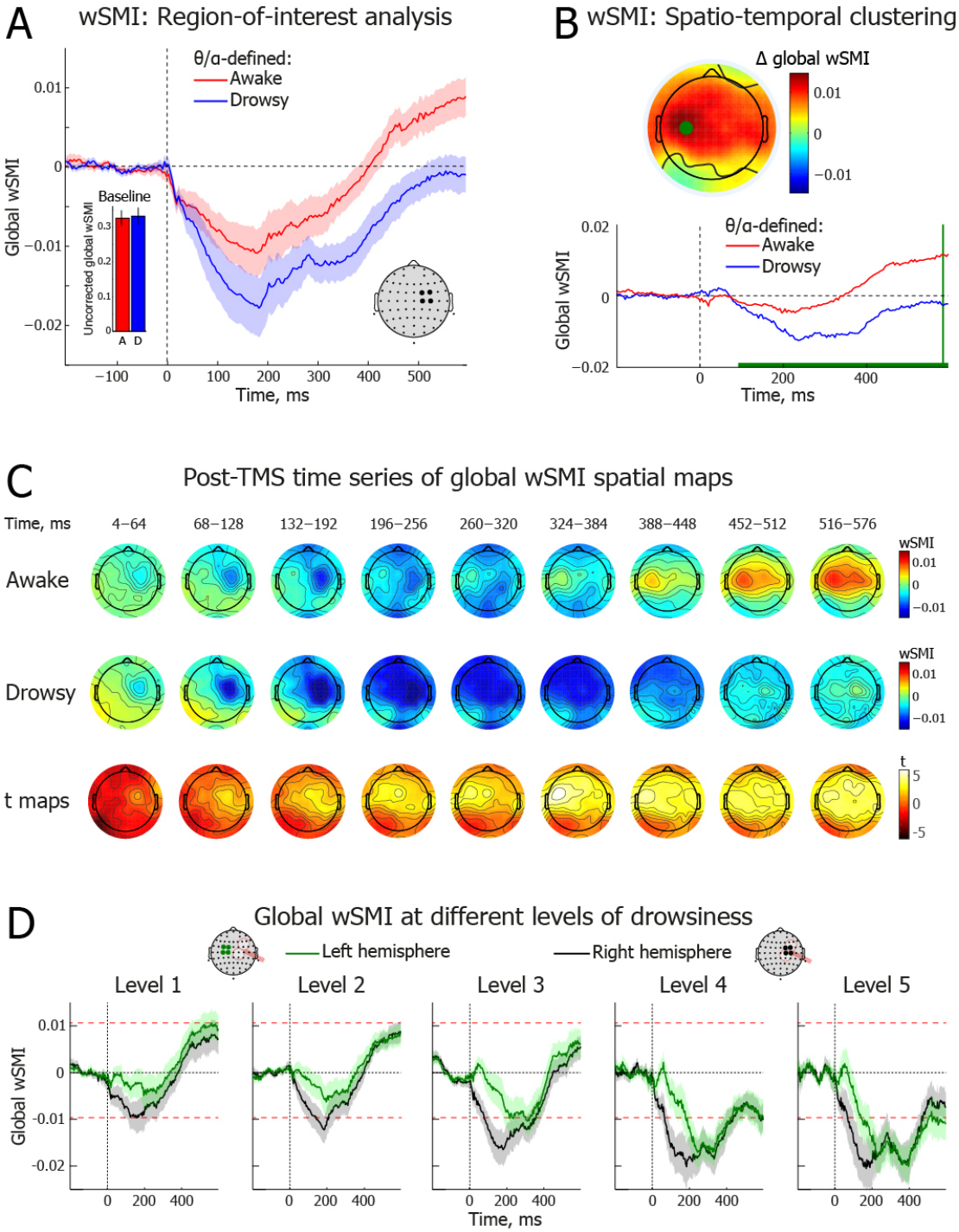

Fig.3. Transcranial magnetic stimulation (TMS) perturbation of electroencephalography (EEG) connectivity as weighted symbolic mutual information (wSMI) in different states of arousal. (A) Time course of wSMI (baseline corrected -400ms to 0ms) averaged over 4 electrodes beneath the TMS coil in the θ/α-defined awake (red) and drowsy (blue) states. Each waveform point represents wSMI calculated over the preceding 200ms time window. A small bar inset on the left represents raw wSMI values over the baseline period in the awake (red) and drowsy (blue) states of arousal. Only responsive trials are included in the analysis shown in this and other subplots. Error shades and bars depict standard error of mean (SEM). **(B)** Data-driven spatiotemporal clustering of wSMI in the 0-600ms time window post TMS between θ/α-defined awake (red) and drowsy (blue) states shows significant

differences between states at 92-596ms time window (cluster peak: 584ms, t = 13409, p = 0.002). Green horizontal line depicts significant differences. The waveforms are from the largest difference between arousal states electrode (green dot). The black contours within the map reveal electrodes with a significant difference (cluster). Green vertical line shows peak time of the largest difference between awake and drowsy states and matches the topographical voltage map. **(C)** Time series of topographic distribution of TMS-locked global wSMI values in the θ/α-defined awake (top) and drowsy (middle) states, and their t-maps difference (bottom). **(D)** Dynamics of wSMI waveforms across Drowsiness Levels 1-5 (wSMI averaged over 4 electrodes beneath the TMS coil in the right hemisphere (black), as well as in the corresponding electrodes in the non-stimulated left hemisphere (green)). Horizontal red dashed lines delineate wSMI peak minimum and maximum in Drowsiness Level 1. Error shades depict SEM.

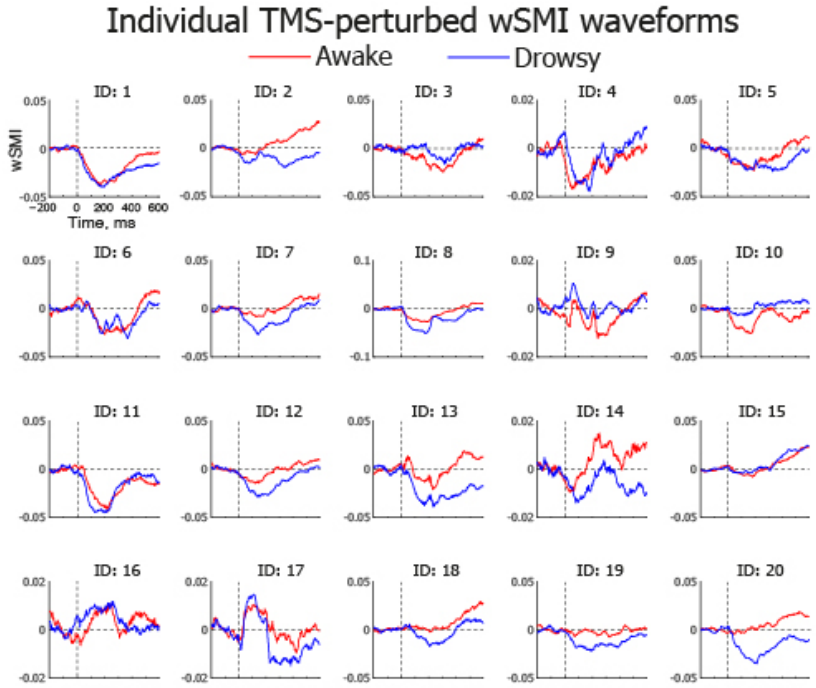

Fig. S8. Individual transcranial magnetic stimulation (TMS)-perturbed weighted symbolic mutual information (wSMI) waveforms in θ/α-defined awake and drowsy states. wSMI waveforms averaged across 4 EEG electrodes within a region-of-interest (ROI) beneath the TMS coil. Awake (red) and drowsy (blue) conditions are depicted separately for each individual (N=20).

Complementary data-driven spatio-temporal clustering revealed higher global wSMI in awake compared to drowsy state in all regions except occipital, with a cluster peak in the contralateral motor region (Fig 3B). While a complex pattern of simultaneous inhibition and facilitation of connectivity emerged in the wake state, global informational disconnection was observed in drowsy trials (Fig 3C). Higher information exchange in the contralateral motor region could be related to the preparatory activity of the networks engaged to respond(*33*, *34*), and/or to TMS-triggered changes in interhemispheric excitability(*35*, *36*). Analysis of the Drowsiness Levels showed the decrease starts in Level 3, with even lower

information sharing in Level 4 (Fig 3D). Thus, our results demonstrate substantial decrease of cortical information connectivity, previously linked to unconscious states(*30*), in individuals who remained conscious and responsive. In other words, sleep-related decrease of global information sharing begins earlier than previously thought.

After establishing arousal-dependent modulation of neurophysiological processes (MEP, TEP, wSMI), we addressed the behavioral response dynamics and related neural processes. A lack of behavioral reactivity is a classic hallmark of sleep(*37*), with a slowing of reaction times (RT) indexing the change of alertness(*21*, *22*, *38*). As predicted, RT lengthened in θ/α-defined drowsy trials (M_{median} =1290 ms, SD=254 ms) compared to awake trials (M_{median}=1170 ms, SD=216 ms) in 19 out of 20 participants ($t_{(19)}$=6.11, p=0.000007, d=0.89) (Fig 4A). Drowsiness Level analysis revealed a clear RT increase (Mann-Kendall trend test: z=4.28, p=0.000018, tau=0.7) (Fig 4B). The speed of processing decreased when spontaneous awake α oscillatory activity became minimal (Drowsiness Level 3), coinciding with a decrease of information sharing (wSMI), thereby suggesting a common pattern of behavior and information sharing dynamics in the process of falling asleep.

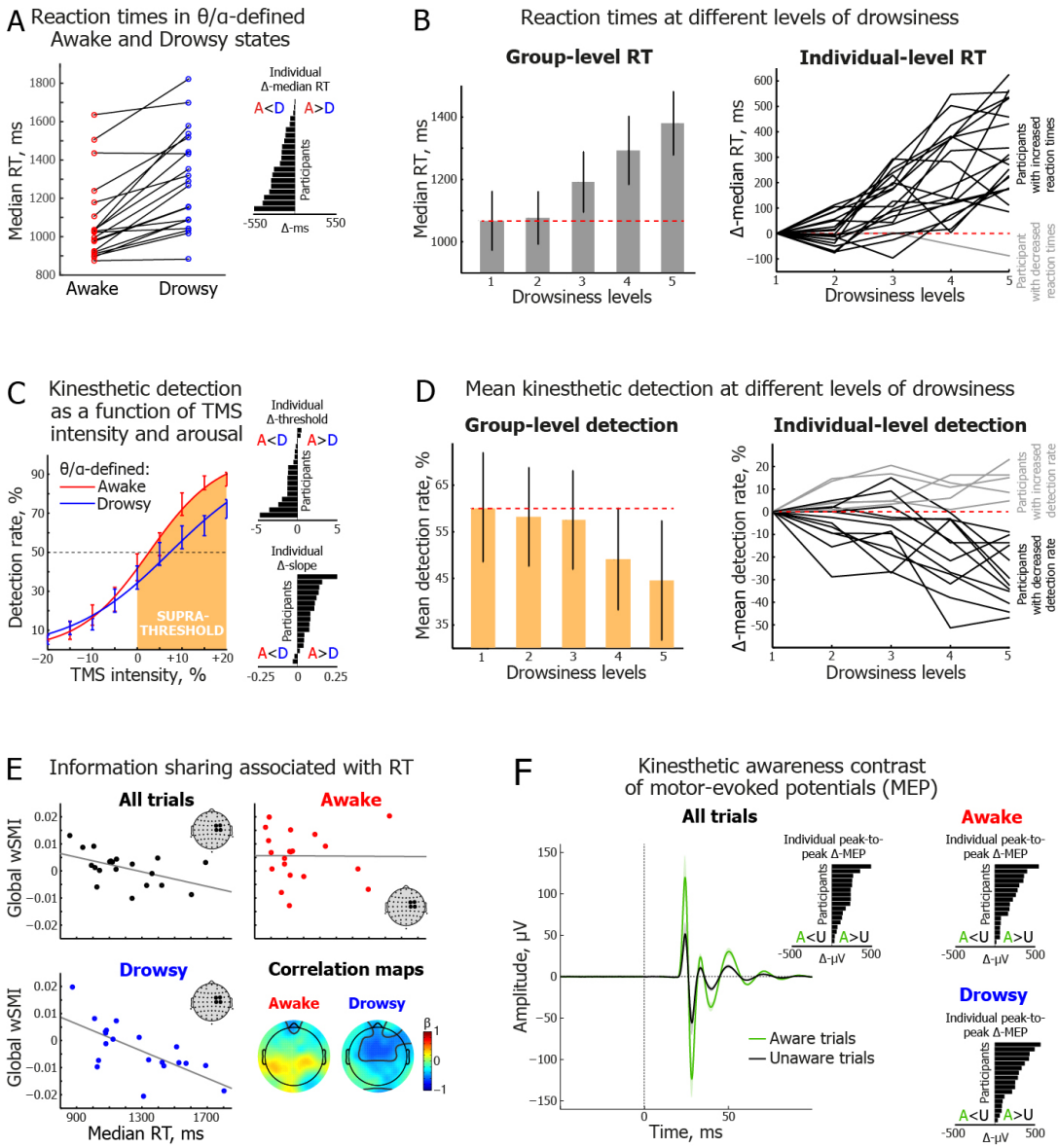

Fig. 4. Behavioral findings in different states of arousal. (A) Median reaction times (RT) in θ/α-defined awake (red) and drowsy (blue) conditions. Inset depicts individual median RT difference (Awake-Drowsy) with participants as individual bars (ascending order of difference). **(B, left)** Group-level change of median RT across Drowsiness Levels 1-5, error bars are standard error of mean (SEM). Horizontal red dashed line delineates median RT in Drowsiness Level 1. **(B, right)** Individual-level dynamics of median RT across Drowsiness Levels 1-5. Black lines represent participants who had longer RT in Drowsiness Level 5 compared to Level 1 (N=19), grey line the participant with shorter (N=1). **(C)** Group-averaged rate of trials with reported kinesthetic awareness across 9 TMS conditions centered on individual motor threshold (0%). Sigmoidal functions fitted separately to the θ/α-defined awake (red) and drowsy (blue) conditions. Error shades represent SEM. Insets show individual threshold and slope differences (Awake-Drowsy), each bar is a participant. Threshold difference between θ/α-awake and drowsy states not associated with slope difference between states (r=0.06, p=0.81), suggesting possible independent variance of these two behavioral measures of awareness reports. **(D, left)** Group-level change of the percentage of "aware" trials in supra-threshold TMS conditions (see C) across Drowsiness Levels 1-5. Horizontal red dashed line delineates awareness rate in Drowsiness Level 1. **(D, right)**

Individual-level dynamics of the percentage of "aware" trials across Drowsiness Levels 1-5. Black lines for participants with lower rate of "aware" trials in Drowsiness Level 5 vs. Level 1 (N=12), grey lines for those with higher (N=5). **(E)** Scatter plots depict regressions between median RT and information-sharing (wSMI) of the stimulation site in the 401-600ms time window, with all trials (black), only θ/α-awake trials (red), or only θ/α-drowsy trials (blue) analyzed. Topographical maps represent the same regression analysis repeated separately for each electrode. **(F)** Mean motor evoked potential (MEP) amplitude difference between "aware" (green) and "unaware" (black) reports. Inset depicts individual MEP peak-to-peak amplitude difference (Aware-Unaware) with participants represented as individual bars that are sorted in the ascending order. Error shades represent SEM.

The assessment of the relationship between cortical information exchange and the speed of response revealed that wSMI decrease predicts RT increase ($F_{(1,18)}$=6.02, p=0.0245, R^2=0.251, β=-0.501; Fig. 4E). Strikingly, when trials were split between θ/α-defined arousal conditions, wSMI successfully predicted RT in drowsy ($F_{(1,18)}$=12.79, p=0.0022, R^2=0.415, β=-0.645) but not in awake trials ($F_{(1,18)}$=0.003, p=0.959, R^2=0.0001, β=-0.012) (Fig. 4E). Furthermore, the association between RT and wSMI was stronger in drowsy than awake states at a single trial level within individual participants (Fig. S9). Linear regression performed separately for each EEG sensor revealed the predictive wSMI-RT association mainly across frontal and central regions (Fig. 4E). In short, the fronto-central global disconnection preceded and predicted the response dynamics as drowsiness progressed.

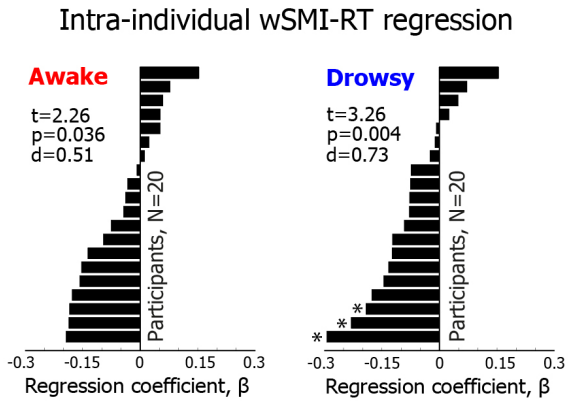

Fig. S9. Intra-individual regression between single-trial weighted symbolic mutual information (wSMI) and reaction times (RT). Regression coefficients β of individual participants represented as bars sorted in ascending order. Analysis was carried out separately for the θ/α-defined awake (red) and drowsy (blue) conditions. One-sample t tests were carried out using individual β values.

Finally, we assessed the arousal-dependent modulation of kinesthetic detection reports. Sigmoidal fitting of kinesthetic awareness reports across 9 TMS intensities revealed that detection threshold increased in θ/α-drowsy compared

to awake states ($t_{(16)}$=3.68, p=0.002, d=0.65), that is, a higher TMS intensity was required to reach the same rate of kinesthetic awareness reports when participants became drowsy (Fig. 4C). Furthermore, a lower slope of sigmoid fit was observed in drowsiness ($t_{(16)}$=4.96, p=0.00014, d=1.05), indicating that kinesthetic detection became "noisier" in the transition from wakefulness to sleep(*39*, *40*) (Fig. 4C). Threshold and slope findings were highly consistent with 15 out of 17 participants showing the same direction of effects (Fig. 4C and Fig. S10). The regional and temporal dynamics of θ/α power revealed widespread arousal-specific modulation of threshold and slope (Fig. S11), again differentiating our findings from the α oscillatory activity commonly associated with attention and sensory gating(*24–26*).

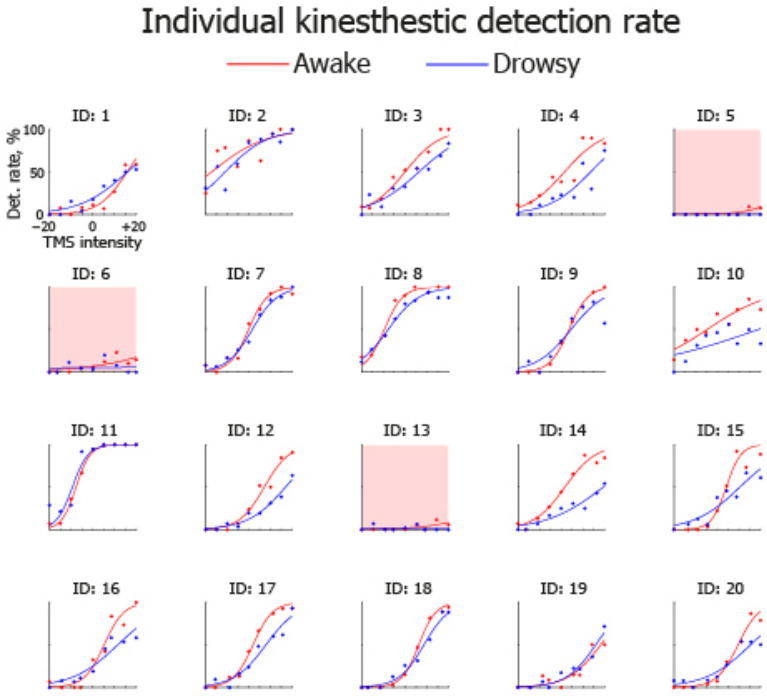

Fig. S10. Individual rate of kinesthetic detection as a function of transcranial magnetic stimulation (TMS) intensity in θ/α-defined awake and drowsy states. Percentage of trials with reported kinesthetic awareness was calculated separately for the awake and drowsy trials across 9 TMS conditions centered on the individual motor threshold (0%). Sigmoidal functions were then fitted to the awake (red) and drowsy (blue) conditions separately for each individual (N=20). Kinesthetic detection rate was too low for participants 5, 6 and 13 to fit individual sigmoidal functions (indexed with pink background).

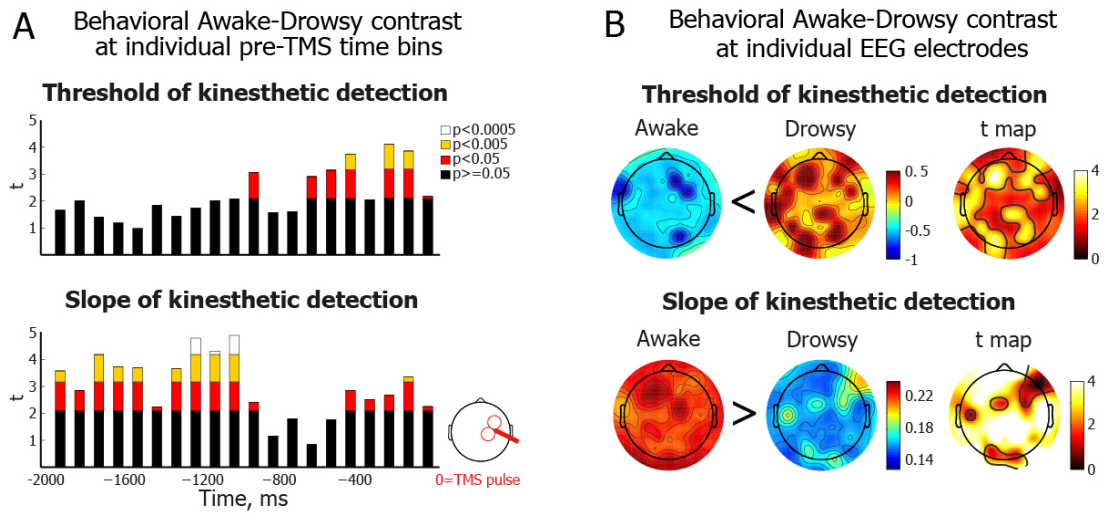

Fig. S11. Temporal and spatial spread of the arousal-dependent modulation of behavioral markers. (A) Difference of the behavioral sigmoid thresholds (top) and slopes (bottom) between θ/α-defined awake and drowsy conditions. Arousal states are measured and contrasted separately for each of the 20 time bins in steps of 100 ms across the -2000-0 ms pre-stimulation time window. Electroencephalography (EEG) spectral power is averaged over all electrodes. **(B)** Difference of the behavioral sigmoid thresholds (top) and slopes (bottom) between θ/α-defined awake and drowsy conditions. Arousal states are measured and contrasted separately for each of the 63 EEG electrodes. EEG spectral power is averaged over -2000-0 ms pre-stimulation time window.

Our findings thus reveal the breakdown of neural cognitive mechanisms supporting conscious awareness when transitioning from an awake to drowsy state of arousal. In particular, individuals lose monitoring sensitivity, as indexed by the increased detection threshold, and their responses become less predictable, revealed by shallower detection slope. Furthermore, the rate of "aware" responses declines across increasing levels of drowsiness. A mean detection rate in supra-threshold TMS conditions revealed a robust linear trend of detection decrease with increasing levels of drowsiness ($F_{(1,16)}=9.59$, $p=0.007$, partial $\eta^2=0.38$) (Fig. 4D).

MEP amplitude differentiated "aware" and "unaware" reports both at a group and a single participant level (Fig. 4F). The same relationship held in both awake and drowsy trials, pointing to some degree of commonality between neural mechanisms underlying kinesthetic awareness in different states of arousal. In addition, there was a tendency towards differential TEP responses as a function of kinesthetic awareness reports (Fig. S12). Thus, in broad terms, early electrophysiological responses (MEP, TEP) predict awareness reports, whereas late information sharing (wSMI) predicts response dynamics, revealing a differential association between specific behavioral and neural measures of task processing.

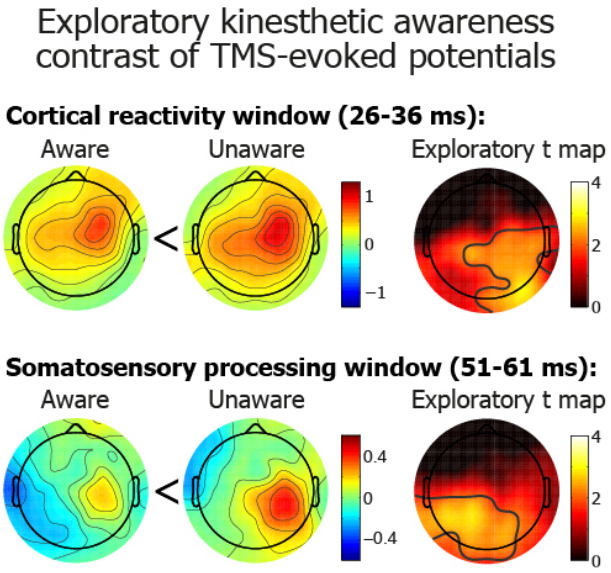

Fig. S12. Transcranial magnetic stimulation (TMS)-locked electroencephalography (EEG) potentials in "aware" and "unaware" reports. Topographical distribution of cortical reactivity (top, 26-36 ms) and somatosensory processing (bottom, 51-61 ms) peak latencies in the aware (left) and unaware (middle) trials. Exploratory t maps (right), i.e. uncorrected for multiple comparisons, indicate regions significantly different between aware and unaware trials ($p<0.05$). However, no significantly different clusters were identified during data-driven spatiotemporal clustering of TMS-locked EEG potentials between aware and unaware trials in the 0-100 ms time window (not shown here).

Our fine-grained analyses revealed the complex dynamics of falling asleep while performing a task (summarised in Fig. 1B and Fig. S13), with each of the assessed neurobehavioral processing stages showing a distinct trajectory towards sleep. In particular, MEP amplitude is highest in Drowsiness Level 4 with a subsequent decrease in Level 5, whereas TEP cortical reactivity peaks and remains stable in Levels 4-5. The amplitude of somatosensory potentials increases with each subsequent stage of drowsiness, whereas RT shows a linear increase from Level 2. The rate of awareness reports continuously decreases across all drowsiness stages, whereas wSMI shows a non-linear pattern of decrease between intermediate Levels 2-4. These multidimensional findings confirm that the brain transitions from one global state (awake) towards another (sleep) as a complex dynamical system; and that the detailed characterization of these processes form the bases to understand the mechanisms underlying how we fall asleep when doing tasks (driving, typing, monitoring, etc.).

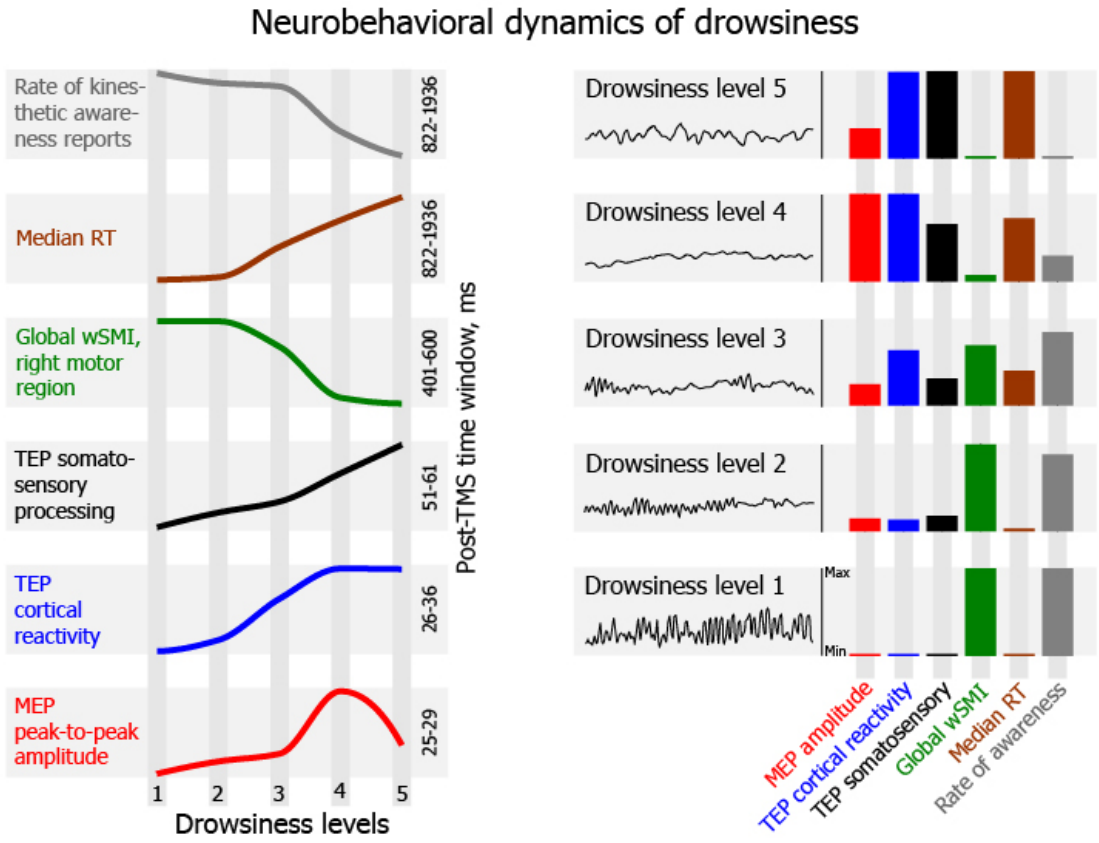

Fig. S13. Dynamical processing of TMS perturbation-kinesthetic detection signatures as a function of Drowsiness Levels. (Left) Key stages of neurobehavioral processing are shown across 5 Levels of Drowsiness. Each measure is standardized between its minimum and maximum values. Interpolant function is fitted to raw measurements using shape-preserving piecewise cubic interpolation (PCHIP). **(Right)** The same neurobehavioral summary measures plotted within each Drowsiness Level. Exemplary EEG scalp recordings (4 sec) indicate electrophysiological patterns typical to a specific level of drowsiness.

Furthermore, we demonstrate that perturbational markers of sleep – facilitation of local cortical reactivity and inhibition of global connectivity – arise in a drowsy state of arousal before participants fall asleep. These findings provide a more complex picture for the neural markers indexing absence of consciousness, challenging previous interpretations(*14–16*, *41*). Contrary to previous reports, we show that participants can remain seemingly conscious and responsive despite a dramatic increase in local reactivity and decrease in global brain connectivity (information-sharing). Thus, local reactivity and global connectivity primarily reflect different levels of arousal and neural capacity to process information and respond rather than the presence or absence of sensory awareness. While the participants were able to report feeling a movement or a muscle twitch in their stimulated hand (Table S1), decreasing levels of arousal substantially modulated the processing of perceptual decisions. Reaction times lengthened, sensory detection thresholds increased and detection slope became shallower. Arguably, such neurocognitive disintegration is one step away from the loss of responsiveness, as we observed the last stages of the fragmentation of

consciousness and cognition preceding behavioral onset of sleep.

We conclude that sleep-related reconfiguration of cortical mechanisms begins while participants are still actively engaged in the monitoring of sensory input. We followed the signal from stimuli to responses in brain and behavior creating a strategy to learn about mechanism underlying cognitive fragmentation. This constitutes a proposal of an experimental framework to study performance in daily arousal changes. While previous research showed complex cognitive processes to persist across drowsiness(*21*) and even in unresponsive NREM sleep(*11*, *42*), we demonstrate some dependencies between physiology and behavior that can guide future endeavor into the mechanism of decision making under arousal stress. Complex neural dynamics indicate that both two global states of consciousness, wake and sleep, are largely overlapping in time. Perceptual processing can thus survive a rapid decrease of arousal, with supporting neural networks flexibly adapting to the rapidly fluctuating background micro-states shifting towards sleep.

References

1. T. Akerstedt *et al.*, *Sleepiness at the Wheel: White Paper* (ASFA & INSV, 2013).
2. D. Leger, The cost of sleep-related accidents: A report for the National Commission on Sleep Disorders Research. *Sleep*. **17**, 84–93 (1994).
3. M. E. Wells, B. V Vaughn, Poor sleep challenging the health of a Nation. *Neurodiagn. J.* **52**, 233–49 (2012).
4. J. Owens, Insufficient sleep in adolescents and young adults: An update on causes and consequences. *Pediatrics*. **134**, e921–e932 (2014).
5. K. R. Rossa, S. S. Smith, A. C. Allan, K. A. Sullivan, The effects of sleep restriction on executive inhibitory control and affect in young adults. *J. Adolesc. Heal.* **55**, 287–292 (2014).
6. T. Shochat, M. Cohen-Zion, O. Tzischinsky, Functional consequences of inadequate sleep in adolescents: A systematic review. *Sleep Med. Rev.* **18**, 75–87 (2014).
7. K. Cervena *et al.*, Spectral analysis of the sleep onset period in primary insomnia. *Clin. Neurophysiol.* **125**, 979–987 (2014).
8. C. R. Burgess, T. E. Scammell, Narcolepsy: Neural mechanisms of sleepiness and cataplexy. *J. Neurosci.* **32**, 12305–12311 (2012).
9. L. Goupil, T. A. Bekinschtein, Cognitive processing during the transition to sleep. *Arch. Ital. Biol.* **150**, 140–154 (2012).
10. P. Grosse, R. Khatami, F. Salih, A. Kuhn, B. U. Meyer, Corticospinal excitability in human sleep as assessed by transcranial magnetic stimulation. *Neurology*. **59**, 1988–1991 (2002).
11. S. Kouider, T. Andrillon, L. S. Barbosa, L. Goupil, T. A. Bekinschtein, Inducing task-relevant responses to speech in the sleeping brain. *Curr. Biol.* **24**, 2208–2214 (2014).
12. J. L. Cantero, M. Atienza, J. R. Madsen, R. Stickgold, Gamma EEG dynamics in neocortex and hippocampus during human wakefulness and sleep. *Neuroimage*. **22**, 1271–1280 (2004).
13. A. G. Casali *et al.*, A theoretically based index of consciousness independent of sensory processing and behavior. *Sci. Transl. Med.* **5**, 1–10 (2013).
14. M. Massimini *et al.*, Breakdown of cortical effective connectivity during sleep. *Science.* **309**, 2228–2232 (2005).
15. M. Massimini, F. Ferrarelli, S. Sarasso, G. Tononi, Cortical mechanisms of loss of

consciousness: Insight from TMS/EEG studies. *Arch. Ital. Biol.* **150**, 44–55 (2012).
16. G. Tononi, M. Massimini, Why does consciousness fade in early sleep? *Ann. N. Y. Acad. Sci.* **1129**, 330–334 (2008).
17. L. De Gennaro *et al.*, Neurophysiological correlates of sleepiness: A combined TMS and EEG study. *Neuroimage*. **36**, 1277–1287 (2007).
18. P. Manganotti, G. Fuggetta, A. Fiaschi, Changes of motor cortical excitability in human subjects from wakefulness to early stages of sleep: A combined transcranial magnetic stimulation and electroencephalographic study. *Neurosci. Lett.* **362**, 31–34 (2004).
19. P. Manganotti, L. G. Bongiovanni, G. Fuggetta, G. Zanette, A. Fiaschi, Effects of sleep deprivation on cortical excitability in patients affected by juvenile myoclonic epilepsy: a combined transcranial magnetic stimulation and EEG study. *J. Neurol. Neurosurg. Psychiatry*. **77**, 56–60 (2006).
20. P. Manganotti, A. Palermo, S. Patuzzo, G. Zanette, A. Fiaschi, Decrease in motor cortical excitability in human subjects after sleep deprivation. *Neurosci. Lett.* **304**, 153–156 (2001).
21. C. A. Bareham, T. Manly, O. V Pustovaya, S. K. Scott, T. A. Bekinschtein, Losing the left side of the world: rightward shift in human spatial attention with sleep onset. *Sci. Rep.* **4**, 5092 (2014).
22. T. Hori, M. Hayashi, T. Morikawa, in *Sleep Onset: Normal and Abnormal Processes*, R. D. Ogilvie, J. R. Harsh, Eds. (American Psychological Association, Washington, DC, 1994), pp. 237–253.
23. R. D. Ogilvie, The process of falling asleep. *Sleep Med. Rev.* **5**, 247–270 (2001).
24. P. Capotosto, C. Babiloni, G. L. Romani, M. Corbetta, Frontoparietal cortex controls spatial attention through modulation of anticipatory alpha rhythms. *J. Neurosci.* **29**, 5863–5872 (2009).
25. H. van Dijk, J.-M. Schoffelen, R. Oostenveld, O. Jensen, Prestimulus oscillatory activity in the alpha band predicts visual discrimination ability. *J. Neurosci.* **28**, 1816–23 (2008).
26. V. Romei *et al.*, Spontaneous fluctuations in posterior α-band EEG activity reflect variability in excitability of human visual areas. *Cereb. Cortex*. **18**, 2010–2018 (2008).
27. R. Huber *et al.*, Human cortical excitability increases with time awake. *Cereb. Cortex*. **23**, 332–338 (2013).
28. R. C. Josiassen, C. Shagass, R. A. Roemer, S. Slepner, B. Czartorysky, Early cognitive components of somatosensory event-related potentials. *Int. J. Psychophysiol.* **9**, 139–149 (1990).
29. J. R. King *et al.*, Information sharing in the brain indexes consciousness in noncommunicative patients. *Curr. Biol.* **23**, 1914–1919 (2013).
30. J. D. Sitt *et al.*, Large scale screening of neural signatures of consciousness in patients in a vegetative or minimally conscious state. *Brain*. **137**, 2258–2270 (2014).
31. A. Canales-Johnson *et al.*, Integration and differentiation of neural information dissociate between conscious percepts. *bioRxiv* (2017) (available at https://doi.org/10.1101/133801).
32. E. Hesse *et al.*, Early detection of intentional harm in the human amygdala. *Brain*. **139**, 54–61 (2016).
33. M. P. Deiber, V. Ibañez, N. Sadato, M. Hallett, Cerebral structures participating in motor preparation in humans: a positron emission tomography study. *J. Neurophysiol.* **75**, 233–247 (1996).
34. K. Sakai, R. E. Passingham, Prefrontal interactions reflect future task operations. *Nat. Neurosci.* **6**, 75–81 (2002).
35. A. Salerno, M. Georgesco, Interhemispheric facilitation and inhibition studied in man with double magnetic stimulation. *Electroencephalogr. Clin.*

Neurophysiol. - Electromyogr. Mot. Control. **101**, 395–403 (1996).
36. Z. Ni *et al.*, Two phases of interhemispheric inhibition between motor related cortical areas and the primary motor cortex in human. *Cereb. Cortex*. **19**, 1654–1665 (2009).
37. N. Kleitman, Sleep. *Physiol. Rev.* **9**, 624–665 (1929).
38. W. T. Liberson, C. W. Liberson, in *Recent Advances in Biological Psychiatry, Vol VIII*, J. Wortis, Ed. (Plenum Press, New York, 1966), pp. 295–302.
39. G. E. Legge, D. Kersten, A. E. Burgess, Contrast discrimination in noise. *J. Opt. Soc. Am. A.* **4**, 391–404 (1987).
40. K. A. May, J. A. Solomon, Four theorems on the psychometric function. *PLoS One*. **8** (2013), doi:10.1371/journal.pone.0074815.
41. C. Koch, M. Massimini, M. Boly, G. Tononi, Neural correlates of consciousness: progress and problems. *Nat. Rev. Neurosci.* **17**, 307–321 (2016).
42. T. Andrillon, A. T. Poulsen, L. K. Hansen, D. Léger, S. Kouider, Neural markers of responsiveness to the environment in human sleep. *J. Neurosci.* **36**, 6583–6596 (2016).

Online Methods and Materials

Participants

20 participants (7 male; mean age 23.7; age range 21-33) signed informed consent and took part in the study. All participants were screened for contraindications to transcranial magnetic stimulation (TMS)(*43*) and inclusion criteria included being 18 to 40 years old, having no history of hearing impairment or injury and no neurological or psychiatric disorders. All participants were right handed, which was assessed with the Edinburgh Handedness Scale(*44*). The mean handedness index was 0.79 (SD=0.19; range 0.3 to 1). Aiming to recruit volunteers who are likely to become drowsy and fall asleep in a laboratory environment during daytime, potential participants were also screened with the Epworth Sleepiness Scale (ESS)(*45*). The mean ESS score was 9.4 (SD=4.3), which indicates that most of the participants were very likely to fall asleep in a situation of prolonged inactivity.

The experimental protocol was approved by the Medical Research Ethics Committee of the University of Queensland and the study was carried out in accordance with the Declaration of Helsinki. Participants were recruited through the electronic volunteer database of the School of Psychology, University of Queensland. They received $30 for taking part in the study. There were no adverse reactions to TMS.

For the analysis of kinesthetic reports, three participants were excluded because of very low rate of "aware" trials (3.8-17.2 %) even at the highest TMS intensities (Fig. S10), which prevented individual sigmoidal fit to their behavioral data.

Electromyography (EMG)

Surface EMG was recorded from the first dorsal interosseous (FDI) of the left and right hand using disposable 24 mm Ag-AgCl electrodes (Kendall H124SG by Covidien; MA, USA). The electrodes were placed in a belly-tendon montage with the reference over the proximal phalanx of the index fingers and a common reference on the right elbow. Raw EMG signals were amplified (×1000) and filtered (20-2000 Hz; 50 Hz notch filter) using a Digitimer NeuroLog system (Digitimer; Hertfordshire, UK). The data were digitised at 5000 Hz using a Power 1401 and Signal (v5) software (Cambridge Electronic Design; Cambridge, UK) and stored for offline analysis on a PC. Throughout the experiment EMG activity was monitored on-line using a digital oscilloscope with a high gain and participants were prompted to relax if activity was observed.

Transcranial magnetic stimulation

TMS was applied to the right motor cortex using a Magstim 200^2 stimulator and 70 mm figure-eight coils (#9925-00; The Magstim Company; Carmarthenshire, UK). The site for stimulation was the point on the scalp over the motor cortex that elicited the largest and most consistent amplitude MEPs from the left FDI. This 'hotspot' was found by initially placing the TMS coil tangentially on the scalp with the handle pointing posteriorly and laterally at ~45° to the sagittal plane and stimulating at a slightly suprathreshold intensity. Once the hotspot had been identified it was marked using an infrared neuronavigation system (Visor 2 by ANT Neuro; Enschede, The Netherlands). A small piece of foam (~ 5) mm thick was then placed under the centre of the TMS coil so that it was not in physical contact with any EEG electrodes. The hotspot was re-marked and the location and orientation of the TMS coil was maintained throughout the testing session with the aid of the navigation system. The navigation accuracy was kept within 5 mm and 5 degrees, but was typically less than 3 mm and 3 degrees. Resting motor threshold was determined using the relative frequency method with a criterion of ≥50 μV (peak-to-peak) MEP amplitude in at least five out of ten consecutive trials(*46–48*). A two-down, one-up staircase was used starting at a suprathreshold intensity. The mean motor threshold was 53.1 % (Min=34, Max=74) of the maximal TMS output intensity.

Electroencephalography

Continuous data were acquired using a 64 channel BrainAmp MR Plus amplifier, TMS BrainCap and Brain Vision Recorder (v1) software (Brain Products; Gilching, Germany). A high chloride abrasive electrolyte gel was used (Abralyt HiCl by Easycap; Herrsching, Germany) and electrode placement corresponded with the International 10-10 system. Data were sampled at 5 kHz with a bandpass filter of DC-1000 Hz and resolution of 0.5 mV (± 16.384 mV). Recordings were referenced online to the left mastoid, and electrode impedance was typically kept below 5 kΩ.

Experimental procedure

Participants were seated in a reclining chair with a leg support. After placing EMG and EEG electrodes, their eyes were blindfolded, the lights in the lab were dimmed, and they were instructed to relax for a few minutes while estimation of individual resting motor threshold was performed. Participants' hands were comfortably supported with pillows. After threshold estimation the main TMS experiment was carried out and participants were reminded to stay relaxed and keep their eyes closed. This time, they were also instructed to pay attention to their left hand and to respond by clicking one of the two mouse keys with their right hand if they felt something, such as a twitch or a touch, in their left hand after each TMS pulse (see Fig 1A). Aiming to unify the response criterion, participants were instructed to avoid guessing and respond positively only if they were certain they felt a sensation; that is, they were guided towards a more conservative response style. Participants were assured that there are no right or wrong answers as we are interested in learning about what they felt. Further, participants were explicitly allowed and encouraged to fall asleep if they wanted to. In a case of 3-5 consecutive unresponsive trials, defined as no response within 6 seconds following TMS, they were gently awakened verbally and reminded to continue the task. Half of the participants responded with the right mouse key if they felt something in their left hand, and with the left mouse key if they felt nothing. For the other half of participants this button mapping was reversed.

During stimulation, nine TMS intensities centred on the individual resting motor threshold (-20%, -15%, -10%, -5%, 0%, +5%, +10%, +15%, +20%) were used. Given that TMS stimulator output intensity is measured in whole numbers from 1 to 100, the calculated percentage from threshold intensity was rounded. This yielded slightly different sized steps from -20% to +20% for some individuals, and this was taken into consideration when fitting sigmoidal functions at a single participant level. 520 trials of single pulse TMS were carried out with an average inter-pulse interval of 9.5 sec and a uniformly distributed random jitter of ±1000 msec; that is, the inter-pulse interval lasted anywhere between 8.5-10.5 sec. A relatively long inter-pulse interval was set to facilitate a natural development of drowsiness as well as to give sufficient time for a return of tonic EMG activity to its baseline level. Aiming to obtain more data around the TMS threshold intensity, the following number of trials were delivered at each TMS intensity: 40 trials (7.7% of a total) at each of the -20%, -15%, -10%, +10%, +15% and +20% intensities; 80 trials (15.4% of a total) at each of the -5% and -5% intensities; 120 trials (23.1% of a total) at 0% intensity (i.e., at the individual resting motor threshold). Trial order was randomized throughout the experiment. TMS pulses were delivered in 8 blocks of 65 trials, with two experimenters holding the coil and monitoring EEG switching their places after each block. A longer break was held after 4 blocks in order to give resting time for participants, to change the heated TMS coil, and to reduce impedance of EEG electrodes if needed. Data collection lasted about 90 minutes. Aiming to control for a possible circadian fluctuation of cortical excitability(*49*), all experiments started at 1 pm when participants tend to be relatively sleepy after having had their lunch. After the experiment, participants filled in the Feedback form asking to report any

sensations they felt in their left hand following TMS.

Data analyses

Behavioral analysis

We aimed to investigate state-modulation of kinesthetic awareness, which was defined as positive behavioral responses or hits, by fitting two different models, a sigmoid function and a linear function, and comparing threshold and slope measures in awake and drowsy trials in each participant separately. A sigmoid function was fitted to the ratio of hits to misses (constrained from 0 to 1 on the *y* axis) across 9 TMS intensities as:

$$F = \frac{1}{1 + e^{-\frac{x-\mu}{s}}}$$

where F is the hits ratio, x is the TMS condition, μ is the threshold value (the TMS condition at the inflection point), and s is inversely proportional to the slope at the threshold. The actual slope of the fitted sigmoid was calculated by fitting a straight line between a point 0.1 above the inflection point and a point 0.1 below it, and finding the slope of this line.

In addition, whilst data from the awake trials had a clear non-linear sigmoid trend, it was noted that this was not always the case for drowsy trials. In order to investigate whether kinesthetic awareness remained non-linear in the drowsy state, the data were also fitted to a linear function:

$$F = mx + c$$

where F is the predicted hits ratio, x is the TMS condition, m is the slope, and c is the point at which the line crosses the y axis.

The goodness of fit was compared for each model in each state of consciousness. As both fitting functions contained the same number of free parameters, 2, the models can be compared using the R^2 values given by:

$$R^2 = 1 - \frac{\sum_x (\gamma_x - f_x)^2}{\sum_x (\gamma_x - \bar{f})^2}$$

where γ_x is the hits ratio measured for each TMS condition x, f_x is the predicted hit ratio given by the model, and $\bar{f}$ is the mean hits ratio measured over all TMS conditions. R^2 varies from 0 to 1 with 1 indicating a perfect fit to the data.

MEP analysis

Peak-to-peak amplitude of motor evoked potentials (MEP) after TMS was calculated for each single trial within 20-45 ms time window using Signal (v5) software (Cambridge Electronic Design; Cambridge, UK). Trials containing phasic

muscle activity in the left FDI channel in the 100 ms before TMS were discarded from the analyses. To assess dynamics of MEP peak-to-peak amplitude across Hori Stages 1-5, responsive trials with MEP amplitude at least twice higher than the peak-to-peak distance in the -100-0 ms baseline window were averaged separately for each Hori stage and each participant. Furthermore, aiming to control for MEP variance as a function of TMS intensity, only three TMS conditions (-5%, 0%, +5%) around individual motor threshold were included in the analysis of MEP changes across Hori stages. A 50 μV cut-off threshold of peak-to-peak amplitude(*46–48*) was used to define the "presence" of MEP response for the sigmoid and linear modelling of data across all 9 TMS intensities (-20%, -15%, -10%, -5%, 0%, +5%, +10%, +15%, +20).

EEG pre-processing and analysis: pre-TMS spectral power

EEG data pre-processing was carried out using EEGlab toolbox for Matlab(*50*), with two separate pre-processing pipelines developed for the analysis of EEG activity before and after TMS. Aiming to calculate EEG spectral power before TMS, the recordings were downsampled to 500 Hz, and then epoched in -4000 ms to -10 ms time segments preceding each TMS pulse. The noisiest epochs were manually deleted, and the most deviant EEG channels were detected with the 'spectopo' function before running the independent component analysis (ICA) for further removal of artefacts (such as eye blinks and saccades, heart beat, muscle noise). ICA was carried out on relatively clean channels only, whereas the noisy channels were recalculated by spherical spline interpolation of surrounding channels after deleting ICA components with artifacts. Data were again manually inspected and several remaining noisy epochs were deleted. On average, 58 trials (11.2%) were discarded per single participant during EMG and EEG pre-processing, and there were on average 462 trials per participant (SD=38, Min=348, Max=513) left for the following analyses.

Spectral power of EEG oscillations during 4 sec preceding TMS was computed using Hilbert transform, set from 1.5 Hz to 48.5 Hz in steps of 1 Hz. Given that estimation of spectral power of slow oscillations can be difficult close to the edges of EEG segments, and we were particularly interested in the spectral power just before TMS pulse, a dummy copy of EEG epochs was created by flipping the left and the right sides of pre-TMS recordings along time axis and the obtained "mirror" data were concatenated with the original pre-TMS data; that is, the time axis of the obtained 7.976 sec EEG epochs was from -4000 ms to -12 ms (original) and then back from -8 ms to -4000 ms (mirror). This way, an abrupt discontinuity was avoided in the time window just before TMS, enabling a more stable estimate of spectral power. After Hilbert transform, the "mirror" part of EEG epochs was deleted, retaining the original pre-TMS window from -4000 ms to -12 ms. To reduce data size, EEG recordings were downsampled to 250 Hz before running Hilbert transform.

EEG measures of drowsiness

Two complementary EEG measures were used to assess the depth of transition

from waking to sleep before each TMS pulse: (1) Hori scoring system of sleep onset EEG(*22*), and (2) a ratio between EEG spectral power of pre-TMS theta and alpha oscillations, which will be referred to as the 'θ/α' measure of drowsiness.

Hori system relies on visual scoring of 4 sec segments of continuous EEG recording(*22*). Its 9 stages of the gradual progression of sleep onset and the slowing down of dominating EEG frequencies range from Hori Stage 1, which refers to the alpha-dominated relaxed wakefulness, to Hori Stage 9, which is defined by the occurrence of complete spindles that coincide with a classic Stage 2 NREM sleep (see Fig 1B). Hori system has been used previously to map dynamic wake-sleep changes in ERP(*51*), EEG spectral power(*52*), reaction times, and the rate of subjective reports of being asleep(*22*). In the present study, Hori stages were visually assessed over 4 sec epochs of pre-TMS period by an experienced sleep researcher, who was blind to the response type (hit, miss, or unresponsive) and the TMS intensity of each particular trial. For scoring purposes, only 19 EEG channels of the standard 20-10 system were used, and EEG recordings were low pass filtered (20 Hz). In the present study, "awake" trials were defined as Hori Stages 1 and 2, and trials scored as Hori Stages 4 and 5 were regarded as "drowsy".

Given that Hori Stages 1 to 4 are marked by a decreasing alpha range activity, whereas Hori Stages 4 to 8 have an increasing theta range activity(*22*), progression of drowsiness can be quantified by a ratio of spectral power of these EEG frequency bands. That is, drowsiness can be defined as a period of time with an increased θ/α ratio of spectral power(*21*). To apply this measure, theta (4.5-7.5 Hz) and alpha (8.5-11.5 Hz) power was first averaged in time from -2000 ms to -12 ms, and a θ/α ratio was then calculated for each trial and electrode. Finally, θ/α ratio was averaged across all electrodes, resulting in a single "sleepiness" number per trial. Trials were then split between 45% of the most "awake" and 45% of the most "drowsy" trials, excluding 10% of the "intermediate" trials.

Importantly, in addition to spontaneous arousal fluctuation, spectral power of EEG pre-stimulus oscillations can reflect attentional sampling and/or sensory gating(*24*–*26*). In these cases, EEG alpha effects are typically restricted to a relatively short pre-stimulus time period of several hundreds of milliseconds(*26*), and to the sensory and/or fronto-parietal regions(*24*, *25*). Expecting that an arousal-related effect would be spatially and temporally widespread and consistent, we repeated analyses by splitting data between awake and drowsy trials separately for each EEG electrode and in 20 short pre-TMS time bins of 100 ms in the -2000-0 ms window.

Pre-TMS level of drowsiness

All participants completed the task and reached the expected level of drowsiness, that is Hori stage 5 or higher, marked by the occurrence and dominance of theta waves. At a group level, a comparable proportion of awake and drowsy trials were obtained (Hori stages 1-2: M=45.17 %, SD=19.92; Hori stages 4-5: M=35.68 %, SD=16.44). However, a large inter-individual variability

was observed with several participants staying mostly in Hori stage 1 and several other participants spending most of the time in Hori stage 5 (see Supplementary Fig 1).

Thus, even though the Hori measure provides absolute electrophysiological signatures of the depth of wake-sleep transition, the θ/α measure was followed aiming to identify equal proportion of awake and drowsy trials within each participant. However, given that the θ/α measure is relative, there was a risk of mislabelling trials for some participants, as it would make a split between "awake" and "drowsy" trials even if all of them would be of Hori Stage 1. Thus, aiming to verify the use of θ/α data splits, we compared these two measures at an individual as well as at a group level. First, we carried out correlation analyses between the two measures of drowsiness within each participant. Second, we compared correlation coefficients against zero, aiming to assess a consistency of an association between the Hori and the θ/α measures at a group level. At an individual level, Hori and θ/α scores were positively and significantly correlated for all 20 participants (individual *rho* ranged from 0.66 to 0.9). Group analysis confirmed a very strong association between these two electrophysiological measures of the wake-sleep transition (one sample *t* test: $t(19)=51.99$, $p<0.000005$), confirming that θ/α could be used reliably to assess the level of drowsiness in the tested sample (see Fig 1C-D).

EEG pre-processing and analysis: TMS-EEG reactivity

Analysis of EEG reactivity to TMS perturbation in the first 50 ms time window requires a perfect alignment of TMS markers with the onset of the actual TMS pulses. Given that some delay and jittering was occurring between a TMS marker and a pulse (M=9.6 ms, SD=1.7 ms), EEG markers indicating TMS intensity were automatically adjusted to the time point of the actual TMS. For this, raw EEG data were segmented ±200 ms around each TMS marker, and global field power (GFP) was calculated as a standard deviation of voltage across all electrodes, resulting in a single time waveform per each TMS marker. Each obtained waveform was baseline corrected to the -200 ms to -50 ms time window and each time sample was transformed to its absolute value. The remaining time window of -49 ms to +200 ms was scanned searching for the first time point where a GFP value five times exceeded the maximal baseline GFP value, which indicated the onset of TMS artifact. The TMS marker was then reallocated to this point in the continuous EEG recording.

The EEG data were processed following ICA-based approach of TMS-EEG artifact cleaning(*53*). First, EEG data were segmented from -1000 ms to 1000 ms around the onset of TMS artifact. Afterwards, the segments were baseline corrected to the mean of -500 ms to -100 ms time window. A line was then fitted to the data from -2 ms to 15 ms, this way deleting the initial TMS-EEG artifact, and the epochs were downsampled to 1000 Hz. The most deviating EEG channels were then detected with the 'spectopo' function and the first round of independent component analysis (ICA) was carried without using noisy channels. After deleting a very distinctive early high amplitude component that reflects TMS-evoked contraction of scalp muscles, EEG data were filtered (1-80 Hz) and

epoched from -400 ms to 600 ms around the onset of TMS marker. Once again, the deviating EEG channels were identified and the second round of ICA was carried out without using noisy channels. Independent components reflecting TMS-EEG decay artifact, eye movements, auditory evoked potentials, 50 Hz line noise, and other sources of noise, were deleted, following which bad channels were recalculated using spherical spline interpolation. The EEG segments were again baseline corrected (-100 ms to -3 ms), and manually inspected deleting several epochs that still contained a visible residual TMS artifact. To account for a within-trial variance, raw voltage of each individual trial was transformed to z-scores using the mean and standard deviation of the baseline period (-100 to -3 ms). Trials were then split into different levels of arousal, following Hori as well as θ/α measures of drowsiness.

To assess changes of EEG reactivity to TMS perturbation in the transition wakefulness to sleep, voltage of four electrodes beneath the TMS coil as a region of interest (ROI) was averaged within each participant. The group-level waveform was then plotted revealing an early TEP peak at 31 ms post TMS. The data were then split between Hori stages and the mean amplitude (±5 ms) of around the peak (26-36 ms) was calculated for each participant and each level of arousal.

ERP dynamics were additionally studied using data-driven spatiotemporal clustering analysis similar to what we previously described(*54*). Awake and drowsy trials were compared in the time windows of interest (15-100 ms) by averaging single-subject data and running group level clustering. Using modified functions of FieldTrip toolbox(*55*, *56*), we compared corresponding spatiotemporal points in individual awake and drowsy trials with an independent samples *t* test. Although this step was parametric, FieldTrip used a nonparametric clustering method(*57*) to address the multiple comparisons problem. *t* values of adjacent spatiotemporal points whose *p* values were <0.05 were clustered together by summating their *t* values, and the largest such cluster was retained. A minimum of two neighboring electrodes had to pass this threshold to form a cluster, with neighborhood defined as other electrodes within a 4 cm radius. This whole procedure, that is, calculation of *t* values at each spatiotemporal point followed by clustering of adjacent *t* values, was repeated 1000 times, with recombination and randomized resampling before each repetition. This Monte Carlo method generated a nonparametric estimate of the *p* value representing the statistical significance of the originally identified cluster. The cluster-level *t* value was calculated as the sum of the individual *t* values at the points within the cluster.

We considered a possibility that a hypothetical arousal-modulation of the contraction of scalp muscles following TMS may have contributed to the arousal-modulation of TEP amplitude. To address this hypothesis, we compared amplitude of ICA component of scalp muscle, which was removed during the first stage of ICA cleaning(*53*), between θ/α-defined awake and drowsy states. No amplitude difference was observed between awake and drowsy trials (see Fig S4), ruling out a possibility that TEP cortical reactivity changes between awake and drowsy states were due to a hypothetical change in the intensity of scalp

muscle contraction.

EEG analysis: weighted Symbolic Mutual Information (wSMI)

In order to quantify the coupling of information flow between electrodes we computed the weighted symbolic mutual information (wSMI)(*29*, *30*). It assesses the extent to which the two signals present joint nonrandom fluctuations, suggesting that they share information. It has three main advantages: (i) it allows for a rapid and robust estimation of the signals' entropies; (ii) it provides an efficient way to detect non-linear coupling; and (iii) it discards the spurious correlations between signals arising from common sources, favoring non-trivial pairs of symbols

For each trial, wSMI is calculated between each pair of electrodes after the transformation of the EEG and LFPs signals into sequence of discrete symbols that are defined by the ordering of k time samples separated in time(*29*). The symbolic transformation depends on a fixed symbol size (k = 3, that is, 3 samples represent a symbol) and a variable τ between samples (temporal distance between samples) which determines the frequency range in which wSMI is estimated. In our case, we choose τ = 8 ms corresponding to the gamma band (at 250 Hz sampling rate).

Then, wSMI was estimated for each pair of transformed EEG and LFPs signals by estimating the joint probability of each pair of symbols. The joint probability matrix was multiplied by binary weights to reduce spurious correlations between signals. The weights were set to zero for pairs of identical symbols, which could be elicited by a unique common source, and for opposed symbols, which could reflect the two sides of a single electric dipole. wSMI is calculated using the following equation:

$$wSMI(X,Y) = \frac{1}{\log(k!)} \sum_{x \in X} \sum_{y \in Y} w(x,y)\, p(x,y) \log\left(\frac{p(x,y)}{p(x)p(y)}\right)$$

where x and y are all symbols present in signals X and Y respectively, $w(x,y)$ is the weight matrix and $p(x,y)$ is the joint probability of co-occurrence of symbol x in signal X and symbol y in signal Y. Finally $p(x)$ and $p(y)$ are the probabilities of those symbols in each signal and $k!$ the number of symbols - used to normalize the mutual information (MI) by the signal's maximal entropy. Temporal dynamics of wSMI was calculated using a 400 ms moving window with 2 ms time step and 96% overlapping, from -400 ms to +600 ms around TMS. Global wSMI was calculated by averaging all electrode pairs for each single electrode, which yielded 63 values that were subjected to spatio-temporal clustering that compared awake and drowsy states. For statistical analyses, wSMI waveforms were baseline corrected to -400 ms to 0 ms time window preceding TMS. As a control analysis, raw global wSMI values averaged across 4 electrodes beneath TMS coil were compared between θ/α-defined awake and drowsy states.

Statistical analysis

Paired samples t test was used to compare behavioral and neural summary measures between θ/α-defined awake and drowsy states. Pooled variance was used to calculate Cohen's d, with 0.2 indicating a small effect size, 0.5 – a medium, and 0.8 – a large effect size(*58*). For a similar comparison of summary measures across Drowsiness Levels 1-5, one way repeated measures ANOVA was carried out with linear as well as non-linear contrasts. Huynh-Feldt correction was used when Mauchly's test indicated violation of the assumption of sphericity. Partial η^2 was calculated as an effect size in ANOVA tests, with 0.01 indicating a small effect size, 0.06 – a medium, and 0.14 – a large effect size (*58*). Linear regression was carried out to assess predictive interaction between measures of interest, such as wSMI and RT. Shapiro-Wilk's test was used assess normality of distribution before running parametric tests. Square-root or lg10 transform was used to normalize skewed data. When transformations failed, non-parametric statistical test were used, such as Wilcoxon signed-rank test instead of a paired samples t test, and Mann-Kendall trend test instead of a one-way repeated measures ANOVA for linear contrast across Drowsiness Levels 1-5. In a case of significant main effect, Bonferroni–Holm multiplicity correction(*59*) of p values was carried out to account for multiple follow up comparisons between baseline Drowsiness Level 1 and following levels. Statistical analyses were carried out using Matlab and IBM SPSS (v22) software packages.

Supplementary results

RT across Drowsiness Levels: Significant trend of RT increase across 5 Drowsiness Levels (Mann-Kendall trend test, see the Main text) was further inspected by the planned comparisons between Level 1 and each of the subsequent Drowsiness Levels. A significant lengthening of RT was observed between Drowsiness Level 1 and Level 3 ($t_{(19)}$=5.03, p=0.00015, d=0.57), Level 4 ($t_{(19)}$=5.72, p=0.000048, d=0.97), and Level 5 ($t_{(19)}$=7.37, p=0.0000024, d=1.4), with no difference between Drowsiness Levels 1 and 2 (d=0.05).

Sigmoidal vs. linear models of kinesthestic awareness reports in awake and drowsy trials: To compare sigmoidal vs. linear models of kinesthetic awareness reports between θ/α-awake and drowsy conditions, coefficient of determination R^2 of sigmoidal and linear functions fitted to the individual rate of aware responses across TMS conditions was calculated separately for the θ/α-awake and drowsy trials. Two-way repeated measures ANOVA was carried out with Models (sigmoidal, linear) and States (awake, drowsy) as independent factors, and R^2 as a dependent measure. There was no main effect of States ($F_{(1,16)}$=0.86, p=0.37, partial η^2=0.05), whereas a significant main effect of Models ($F_{(1,16)}$=22.99, p=0.0002, partial η^2=0.59) and a significant Models x States interaction ($F_{(1,16)}$=8.71, p=0.0094, partial η^2=0.35) were observed. While R^2 of sigmoidal fit was significantly higher than R^2 of linear fit in both awake ($t_{(16)}$=5.43, p=0.000056, d=0.86) and drowsy ($t_{(16)}$=3.03, p=0.008, d=0.34) states, an R^2 difference between sigmoidal and linear fits was larger in awake trials

($t_{(16)}$=2.95, p=0.0094, d=0.64), indicating that interaction between detection rate and signal intensity became relatively more linear in the transition to sleep.

Temporal-hemispheric global wSMI differences between awake and drowsy states: To assess whether hemispherical differences in the dynamics of global wSMI, i.e. an initial post-TMS decrease and a subsequent recovery an increase, are dependent on the level of drowsiness, three-way repeated measures ANOVA was carried out with Hemispheres (left ROI, right ROI), Time (1-200 ms, 201-400 ms, 401-600 ms) and Drowsiness Levels (1-5) as independent factors, and global wSMI as a dependent measure. We observed significant main effects of Hemispheres ($F_{(1,19)}$=20.61, p=0.00022, partial η^2=0.52), Time ($F_{(2,38)}$=14.84, p=0.000017, partial η^2=0.44), and Drowsiness Levels ($F_{(3.15,59.88)}$=9.49, p=0.000024, partial η^2=0.33). Global wSMI was significantly lower in the stimulated right hemisphere site compared to the non-stimulated left hemisphere (p=0.00022). Quadratic contrast of Time conditions indicated a non-linear temporal dynamics of post-TMS global wSMI ($F_{(1,19)}$=17.31, p=0.00053, partial η^2=0.48). Pairwise comparisons revealed a higher wSMI in the latest 401-600 ms time window compared to 1-200 ms (p=0.0074) and 201-400 ms windows (p=0.000032). A significant two-way interaction was observed between Time and Drowsiness Levels ($F_{(8,152)}$=7.49, p=0.00000002, partial η^2=0.28). Pairwise comparisons showed that global wSMI did not differ between 1-200 ms and 201-400 ms time windows, but increased in 401-600 ms window compared to 1-200 ms window in Drowsiness Levels 1-3. A contrary effect was observed in Drowsiness Levels 4-5, with a significant decreased of global wSMI between 1-200 ms and 201-400 ms time windows, but no differences between 1-200 ms and 401-600 ms time windows.

Supplementary references

43. S. Rossi *et al.*, Safety, ethical considerations, and application guidelines for the use of transcranial magnetic stimulation in clinical practice and research. *Clin. Neurophysiol.* **120** (2009), pp. 2008–2039.
44. R. C. Oldfield, The assessment and analysis of handedness: The Edinburgh inventory. *Neuropsychologia*. **9**, 97–113 (1971).
45. M. W. Johns, A new method for measuring daytime sleepiness: the Epworth sleepiness scale. *Sleep*. **14** (1991), pp. 540–545.
46. K. Ikoma, A. Samii, B. Mercuri, E. M. Wassermann, M. Hallett, Abnormal cortical motor excitability in dystonia. *Neurology*. **46**, 1371–6 (1996).
47. A. Samii, E. M. Wassermann, K. Ikoma, B. Mercuri, M. Hallett, Characterization of postexercise facilitation and depression of motor evoked potentials to transcranial magnetic stimulation. *Neurology*. **46**, 1376–1382 (1996).
48. P. M. Rossini *et al.*, Non-invasive electrical and magnetic stimulation of the brain, spinal cord and roots: basic principles and procedures for routine clinical application. Report of an IFCN committee. *Electroencephalogr. Clin. Neurophysiol.* **91**, 79–92 (1994).
49. M. V. Sale, M. C. Ridding, M. A. Nordstrom, Factors influencing the magnitude and reproducibility of corticomotor excitability changes induced by paired associative stimulation. *Exp. Brain Res.* **181**, 615–626 (2007).
50. A. Delorme, S. Makeig, EEGLAB: An open source toolbox for analysis of single-trial EEG dynamics including independent component analysis. *J. Neurosci. Methods*.

134, 9–21 (2004).

51. H. Nittono, D. Momose, T. Hori, Gradual changes of mismatch negativity during the sleep onset period. *Sleep Res. Online*. **2(Suppl.1)**, 287 (1999).
52. H. Tanaka, M. Hayashi, T. Hori, Topographical characteristics and principal component structure of the hypnagogic EEG. *Sleep*. **20**, 523–534 (1997).
53. N. C. Rogasch *et al.*, Removing artefacts from TMS-EEG recordings using independent component analysis: Importance for assessing prefrontal and motor cortex network properties. *Neuroimage*. **101**, 425–439 (2014).
54. S. Chennu *et al.*, Expectation and attention in hierarchical auditory prediction. *J. Neurosci.* **33**, 11194–205 (2013).
55. E. Maris, R. Oostenveld, Nonparametric statistical testing of EEG- and MEG-data. *J. Neurosci. Methods*. **164**, 177–190 (2007).
56. R. Oostenveld, P. Fries, E. Maris, J. M. Schoffelen, FieldTrip: Open source software for advanced analysis of MEG, EEG, and invasive electrophysiological data. *Comput. Intell. Neurosci.* **156869** (2011), doi:10.1155/2011/156869.
57. E. T. Bullmore *et al.*, Global, voxel, and cluster tests, by theory and permutation, for a difference between two groups of structural MR images of the brain. *IEEE Trans. Med. Imaging*. **18**, 32–42 (1999).
58. J. Cohen, *Statistical Power Analysis for the Behavioral Sciences* (Lawrence Erlbaum Associates, New York, NY, ed. 2nd, 1988).
59. S. Holm, A simple sequentially rejective multiple test procedure. *Scand. J. Stat.* **6**, 65–70 (1979).